A&A 563, A13 (2014)
DOI: 10.1051/0004-6361/201323101

Astronomy & Astrophysics

The Na-O anticorrelation in horizontal branch stars

IV. M 22⋆,⋆⋆

R. G. Gratton[1], S. Lucatello[1], A. Sollima[2], E. Carretta[2], A. Bragaglia[2], Y. Momany[1,3], V. D'Orazi[4,5], S. Cassisi[6,7], and M. Salaris[8]

[1] INAF – Osservatorio Astronomico di Padova, Vicolo dell'Osservatorio 5, 35122 Padova, Italy
e-mail: raffaele.gratton@oapd.inaf.it
[2] INAF – Osservatorio Astronomico di Bologna, via Ranzani 1, 40127 Bologna, Italy
[3] European Southern Observatory, 3107 Alonso de Cordova, Vitacura, Santiago, Chile
[4] Department of Physics & Astronomy, Macquarie University, Balaclava Rd., North Ryde, NSW 2109 Sydney, Australia
[5] Monash Centre for Astrophysics, School of Mathematical Sciences, Building 28, Monash University, VIC 3800 Victoria, Australia
[6] INAF – Osservatorio Astronomico di Teramo, via Collurania, 64100 Teramo, Italy
[7] Instituto de Astrofisica de Canarias, La Laguna, 38200 Tenerife, Spain
[8] Astrophysics Research Institute, Liverpool John Moores University, Twelve Quays House, Birkenhead, UK

Received 21 November 2013 / Accepted 14 January 2014

ABSTRACT

We obtained high-resolution spectra for 94 candidate stars belonging to the HB of M 22 with FLAMES. Previous works have indicated that this cluster has split subgiant (SGB) and red giant branches (RGB) and hosts two different stellar populations, differing in overall metal abundance and both exhibiting a Na-O anti-correlation. The HB stars we observed span a restricted temperature range ($7800 < T_{\rm eff} < 11\,000$ K), where about 60% of the HB stars of M 22 are. Within our sample, we can distinguish three groups of stars segregated (though contiguous) in colours: Group 1 (49 stars) is metal-poor, N-normal, Na-poor, and O-rich: our abundances for this (cooler) group match those determined for the primordial group of RGB stars (a third of the total) from previous studies very well. Group 2 (23 stars) is still metal-poor, but it is N- and Na-rich, though only very mildly depleted in O. We can identify this intermediate group as the progeny of the metal-poor RGB stars that occupy an intermediate location along the Na-O anti-correlation and include about 10% of the RGB stars. The third group (20 stars) is metal-rich, Na-rich, and O-rich. This hotter group most likely corresponds to the most O-rich component of the previously found metal-rich RGB population (a quarter of the total). We did not observe any severely O-depleted stars and we think that the progeny of these stars falls on the hotter part of the HB. Furthermore, we found that the metal-rich population is also over-abundant in Sr, in agreement with results for corresponding RGB and SGB stars. However, we do not find any significant variation in the ratio between the sum of N and O abundances to Fe. We do not have C abundances for our stars. There is some evidence of an enhancement of He content for Groups 2 and 3 stars ($Y = 0.338 \pm 0.014 \pm 0.05$); the error bar due to systematics is large, but a consistent analysis of data for several GCs confirms that stars in these groups within M 22 are probably overabundant in He. We conclude that on the whole, our results agree with the proposition that chemical composition drives the location of stars along the HB of a GC. Furthermore, we found a number of fast rotators. They are concentrated in a restricted temperature range along the HB of M 22. Fast rotating stars might be slightly less massive and bluer than slowly rotating ones, but other interpretations are possible.

Key words. stars: abundances – stars: evolution – stars: Population II – globular clusters: general – globular clusters: individual: M 22

1. Introduction

Low-mass core He-burning stars show a wide distribution in the colour-magnitude diagram of globular clusters (GCs) along the so-called horizontal branch (HB). This distribution primarily reflects variations in masses and the chemical composition of stars, with a minor but non-negligible part being played by the stars' evolution off their initial location on the zero age horizontal branch (ZAHB). Full understanding of the reasons individual stars occupy a given position along the ZAHB has still not been achieved, probably because several different mechanisms are involved simultaneously. This constitutes the "second parameter problem" (Sandage & Wildey 1967; van den Bergh 1967), and the first parameter is metallicity, which is responsible for most of the observational variance (Sandage & Wallerstein 1960; Faulkner 1966). Important progress has been made thanks to the understanding that significant star-to-star variations can be expected in the helium content within individual GCs, which are made of different stellar populations (see Ventura et al. 2001; Bedin et al. 2004; D'Antona et al. 2005; Norris 2004; Piotto et al. 2005; following much earlier suggestions by e.g. Rood 1973; and Norris et al. 1981). Older and/or He-richer stars are expected to leave the main sequence phase with lower masses. If they lose a similar amount of mass as younger and/or He-normal stars along the RGB, they are expected to be less massive, that is, bluer, when on the HB. There is a broad correlation between extension of the HB and properties very likely related to He abundances, such as the extension of the Na-O anti-correlation (Na-rich and O-poor stars are expected to be more He-rich than Na-poor and O-rich ones; Carretta et al. 2007), both driven mainly by the total mass of the GCs (Recio-Blanco et al. 2006).

A few years ago, we (Gratton et al. 2010; see also Dotter 2013 for a review of this and later contributions) presented a quite extensive re-analysis of the distribution of stars along the

⋆ Based on observations collected at ESO telescopes under programmes 087.D-0230 and 091.D-0151.

⋆⋆ Tables 3–6 are only available at the CDS via anonymous ftp to cdsarc.u-strasbg.fr (130.79.128.5) or via http://cdsarc.u-strasbg.fr/viz-bin/qcat?J/A+A/563/A13

Table 1. Summary of results on Na-O abundances along the HB in various clusters.

Cluster	Red HB	Blue HB
47 Tuc	[Na/O] correlates with colour	
(Gratton et al. 2013)	(increases as B-V decreases)	
NGC 1851	Mostly O-rich/Na-poor	Na-rich/O-poor
(Gratton et al. 2012a)	10−15% Na-rich, moderately O-poor	(Na-O anticorrelation)
	Mostly descendants from b-SGB	Mostly descendants from f-SGB
NGC 2808	O-rich	Moderately O-poor
(Gratton et al. 2011)	Spread Na (correlated with colour)	Moderately Na-rich
M 5	Na-poor, O-rich	Na-O anticorrelation
(Gratton et al. 2013)		Most stars with abundances similar to RHB stars

HB of several tens GCs and found that a combination of variations in age (from cluster-to-cluster) and He-content (from star-to-star within a cluster), added to metallicity, may indeed explain most of the variance in the HB morphology. This was achieved by adopting a simple universal relation between the total mass lost along the RGB and metallicity, with a small (but not negligible) star-to-star random contribution (one-two hundredths of solar masses, about 10% of the total mass lost along the RGB). The presence of this last random term most likely implies that even if the scenario considered by Gratton et al. were broadly correct, something still needs to be added in order to achieve very accurate predictions. Potential candidates, whose importance has not yet been well established, include variations in the CNO/Fe abundance ratio, core rotation, and binarity. The list of potential parameters is even longer, see Fusi Pecci & Bellazzini (1997) and Catelan (2009) for more comprehensive summaries.

A corollary of the star-to-star He abundance variations explanation for the distribution of stars along the HB of an individual GC is that there should be correlations between temperatures and chemical abundances, only partly fuzzed by evolution off the ZAHB. Such correlations can be retrieved through spectroscopy of HB stars. However, spectra of HB stars are difficult to analyse. Ever since the pioneering work of Peterson (1983) we know that rotation can be present on the BHB. Furthermore, abundances for stars hotter than about 11 000 K (the so-called Grundahl-jump, Grundahl et al. 1999) are heavily affected by diffusion and radiative levitation (e.g. Behr et al. 1999; Mohler 2001; Moni Bidin et al. 2006).

Villanova et al. (2009) first tried to connect spectroscopic determinations of the composition of stars along the HB of NGC 6752 with the multiple population scenarios and were also able to obtain information about He, though with non-negligible error bars, finding a low He abundance consistent with the cosmological value, as expected for the kind of stars observed. In fact, He-rich stars are expected to be hotter than the Grundahl-jump in most old and metal-poor GCs in order to avoid too bright HB's at the RR Lyrae colours, as has been known for several decades (see e.g. Iben 1968; Cassisi et al. 2003; Salaris et al. 2004; and the review by Catelan 2009). Two other papers on M 4 (Marino et al. 2011a; Villanova et al. 2012) have confirmed what has been found by Villanova et al. (2009): red HB stars (RHB: that is, stars redder than the RR Lyrae instability strip) are Na-poor and O-rich, while BHB stars are Na-rich and O-poor. Furthermore, the observed BHB stars of M 4, which are amongst the warmest in that cluster, are more He-rich than the stars observed in NGC 6752.

In this series of papers we present the analysis of wide samples of HB stars for a few important GCs. Table 1 gives a summary of main results obtained in published papers. In Gratton et al. (2011) we considered NGC 2808; as in M 4, which has similar metallicity, RHB stars are O-rich, but they show a spread in Na abundances correlated with temperature. Blue HB stars cooler than the Grundahl-jump are (moderately) O-poor and Na-rich. These results have been confirmed by Marino et al. (2014) using higher signal-to-noise ratio (S/N) spectra, from which they also derived He abundances and finding quite a high value of $Y \sim 0.34 \pm 0.01 \pm 0.05$ for BHB stars. Even He-richer stars should be present, but they should be hotter than the Grundahl-jump (D'Antona et al. 2005), so this cannot be verified directly. Gratton et al. (2012a) studied NGC 1851, which is a complex GC with a split SGB (Milone et al. 2009), two populations slightly differing in their Fe-content (Carretta et al. 2010, 2011), and related to the bright (b-)SGB (metal-poor) and the faint (f-)SGB (metal-rich: Gratton et al. 2012b), and two distinct Na-O anti-correlations (Carretta et al. 2010, 2011). Also the bimodal HB of NGC 1851 is complex, with the RHB stars separated into two groups. The vast majority are O-rich and Na-poor, while about 10−15% are Na-rich and moderately O-poor. A separate Na-O anti-correlation is seen among BHB stars. We suggested that most BHB stars descend from the f-SGB stars and are older and that most RHB stars descend from the b-SGB ones and are younger, but the correspondence is probably not one-to-one. Finally, 47 Tuc and M 5 were discussed in Gratton et al. (2013). The cluster 47 Tuc is a simpler case, with a clear correlation between the location on the HB and the Na and O abundances (i.e. like M 4). Instead, while RHB stars in M 5 are invariably Na-poor and O-rich, the case is more complex for BHB stars, and the lack of a tight correlation between colours and chemical composition for these stars requires some additional mechanism to explain observations.

In this paper we focus on M 22 (=NGC 6656), a very intriguing GC. Marino et al. (2009, 2011a,b) show that there are two populations in this cluster with different values of [Fe/H], robustly confirming findings based on calcium (Da Costa et al. 2009; Lee et al. 2009). The two populations can be identified with the two SGBs (Marino et al. 2009, 2012): the metal-poor RGB population is the descendant of the b-SGB, and the metal-rich one of the f-SGB. Both populations display a separate Na-O anti-correlation. The metal-rich population also appears to be much richer in s-process elements, and Marino et al. (2012) suggest that it is also richer in the sum of the CNO elements, a fact that could help explain the split SGB since at a given age and metallicity, stars richer in CNO elements are fainter on the SGB. These properties of M 22 closely resemble those of NGC 1851, but its predominantly blue HB does not present the striking bi-modality seen in the latter, maybe because of the different metal content ([Fe/H] = −1.70 for M 22 vs. [Fe/H] = −1.18 for NGC 1851: Harris 1996). Two recent papers have studied the HB of M 22: a high dispersion study of seven among the coolest non-variable HB stars of M 22 has been presented by

Marino et al. (2013), while Salgado et al. (2013) employed low-resolution blue spectra to measure masses over a large portion of the HB. Marino et al. (2013) found that all these stars are Ba-poor and Na-poor. This favours the hypothesis that the position of a star along the HB is strictly related to the chemical composition and that these stars all belong to the first (Na-poor and He-normal) portion of the metal-poor population of M 22. This agrees with an analysis of the whole colour-magnitude diagram by Joo & Lee (2013), who identified BHB stars with the metal-poor population and the extreme BHB stars with the metal-rich one. According to these last authors, a large difference in helium abundance ($Y = 0.23$ to 0.32) is required to explain the HB. Our analysis allows extending the study of Marino et al. (2013) to a much larger sample of HB stars.

Section 2 presents the observations and data reduction, explaining how they differ from what has been done for the other GCs studied in this series. Derivation of the atmospheric parameters and detail of the abundance analysis are given in Sect. 3. Section 4 presents the results and assignment of the stars to three different populations based on a statistical cluster analysis. Section 5 presents a discussion of the HB of this cluster based on these results and on a comparison with evolutionary models. Conclusions are drawn in Sect. 6.

2. Observations

The present analysis is based on spectra obtained with the GIRAFFE spectrograph of the FLAMES multi-object facility at the VLT UT2 Kueyen telescope (Pasquini et al. 2004). FLAMES was used in MEDUSA mode, with individual fibres pointed to stars or empty sky positions. Spectra were obtained with three different set ups: HR03 (wavelength range 4033−4201 Å, resolution $R \sim 24\,800$), HR12 (wavelength range 5821−6146 Å, resolution $R \sim 18\,700$), and HR19A (wavelength range 7745−8335 Å, resolution $R \sim 13\,867$). The HR12 and HR19A set ups were selected to allow observations of the strongest features of Na I (the D resonance doublet) and O I (the 7771−74 Å high excitation triplet) observable in metal-poor BHB stars, other lines of the same elements being too weak in such stars. High excitation lines of N I and Mg II are also present in these spectral regions. To unambiguously separate the two main populations of M 22 (the metal-poor one, related to the bright SGB, and the metal-rich one, to the faint SGB), we then asked for additional observing time with the HR03 set up, giving access to several strong Fe I features and the resonance line of Sr II at 4077 Å, which is the strongest feature of an element produced by n-capture processes. In addition, this spectral region provides data on Mg I, Si II, Ti II, Fe II, and Hδ, which could be used to derive a reddening-free temperature index. This also allowed solving ambiguities related to differential reddening when analysing the spectra. The journal of observations is in Table 2.

We focussed our attention on the BHB between the blue edge of the instability strip (at an effective temperature of about 7800 K) and the Grundahl jump (at an effective temperature of 11 000 K), though our faint limit actually is slightly brighter than the Grundahl jump. Cooler stars, most of them RR Lyrae variables, were avoided because scheduling their observation at the appropriate phases required for the analysis would have been impractical. Hotter stars were also not included because their abundances are affected by the impact of microscopic diffusion and radiative levitation. When we considered the photometry by Monaco et al. (2004) over 424 bona fide HB stars, we counted 28 stars (that is 7%) with $(B - V)_0 > 0.15$, hence within the instability strip; 221 stars (52%) with $(B - V)_0 < 0.15$ and with $M_V < 14.8$, that is, within the range of our spectroscopic sample; and 175 stars (41%) fainter stars. Counting stars on the *vby* photometry of the cluster from Richter et al. (1999), kindly provided by the authors, we found that in their photometry (which covers an area of M 22 similar to the one we are considering here) there are 71 stars (that is, 32% of total) bluer than the Grundahl jump, 138 stars (61% of total) in the observed range, and 16 redder stars (7% of total). The small difference between star counts of Monaco et al. and Richter et al. most likely depends on different definition of the photometric limits. These numbers (and their uncertainties) should be taken into account when interpreting our results in terms of the stellar populations of M 22 (see Sect. 5).

We were able to point fibres on 94 stars, selected from the photometry by Monaco et al. (2004). The location of these stars on the colour-magnitude diagram is shown in Fig. 1. The stars were selected to have no neighbour within 2 arcsec that are brighter than $M_{\rm target}+2.5$ mag than the target star. One of the stars (#130 on our notation) was revealed to be a field star from its discrepant radial velocity. It also has much stronger lines than the stars of M 22. An additional star (#114 on our notation), though

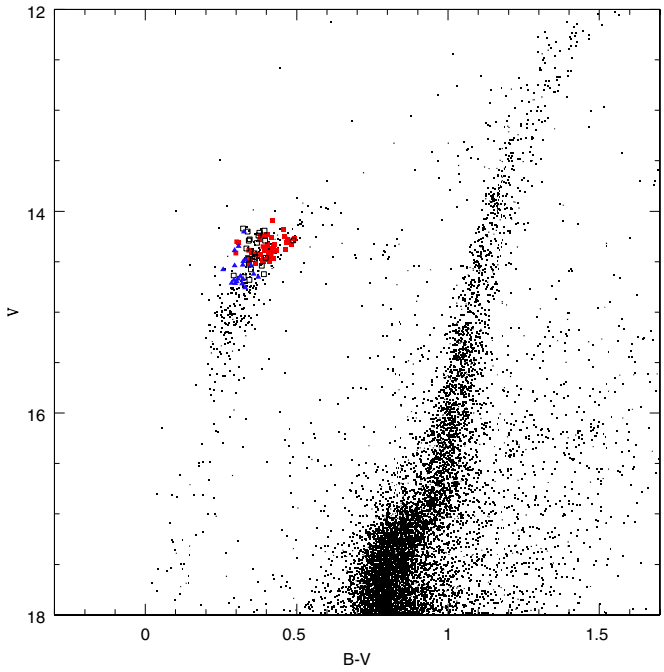

Fig. 1. $(V, B-V)$ colour–magnitude diagram of M 22 from Monaco et al. (2004). Different symbols are for stars of different groups (see Sect. 4): Group 1: red filled squares; Group 2: black open squares; Group 3: blue filled triangles. Dots are the stars not observed in this paper.

Table 2. Observing log.

Set up HR	Date	UT Start	Exp. time (s)	Airmass	Seeing (arcsec)
3	2013-04-25	05:27:57	2400	1.53	1.14
3	2013-04-25	06:09:42	2400	1.30	1.25
3	2013-07-06	07:49:52	2400	1.47	2.19
3	2013-07-10	02:56:02	2400	1.04	0.92
3	2013-08-01	03:12:40	2400	1.01	0.91
3	2013-08-01	04:37:01	2400	1.12	0.77
12	2011-09-11	03:16:50	1500	1.41	1.29
19A	2011-06-29	07:21:31	2500	1.21	1.84

clearly a cluster member, is a small amplitude (0.04 mag) variable (star KT-51 in the Kaluzny & Thompson 2001 list). When analysed as the other programme stars are, it yielded odd results, very likely due to large temperature variations during our observations, which span a few years. All remaining observed stars yielded consistent radial velocity and are likely members of M 22, whose radial velocity of −146.3 km s^{-1} (Harris et al. 1996) sets them far from expectations for most field stars. Fourteen fibres were pointed to empty sky locations.

We collected photometric data for the programme stars from various sources: broad band *BVI* photometry based on data acquired with the WFI camera at the ESO 2.2 m telescope (Monaco et al. 2004); *vby* Strömgren photometry by Richter et al. (1999), kindly provided by the authors; and 2MASS *JHK* photometry (Skrutskie et al. 2006). These photometric data were dereddened using the reddening map by Monaco et al. (2004). Relevant data are listed in Table 3. While we do not list errors for individual stars for the *vby* photometry, paper, upper limits for the total photometric errors are 0.015 mag for V, 0.019 mag for $(b-y)$, and 0.029 mag for m_1, according to Richter et al. (1999).

Exposure times were set to provide $S/N \sim 50$ for all the observed spectral ranges. Observations longer than 45 min were then split into several visits that were performed over several months. Spectra were extracted and calibrated using the ESO FLAMES/GIRAFFE pipeline v 2.11.1, running under GASGANO environment[1]. Sky subtraction, combination, continuum normalization, and shifting to rest frame were performed with IRAF[2]. A median of the sky spectra was obtained. Different spectra for the same star were cross correlated with respect to the first exposure and brought to common radial velocity before being combined using the median over different exposures (the spectra have similar shapes and flux levels); we then applied the barycentric correction of the first spectrum. Shift to rest wavelength was done using the radial velocities measured in the spectra. A normalisation was done on the spectra using CONTINUUM task within IRAF with a third-order Legendre function.

2.1. Radial velocities

We measured radial velocities from the co-added spectra obtained with individual set ups (see Table 4). They were measured using Gaussian fitting to the position of three to eight lines in each spectrum and the same lines were used for all stars. Since very few spectral lines are detectable, radial velocities have quite large errors: comparison of different spectra yields typical errors of ±2.4 km s^{-1} for set-up HR03 and HR19A (see Fig. 2), while typical errors are twice as large for set-up HR12. Weighted averages have typical errors of ±1.7 km s^{-1}, fully adequate both as a membership criterion and for comparison of the scatter we obtain within different groups of stars with the overall dispersion of the radial velocities for the cluster, which we measured at 7.7 ± 0.8 km s^{-1} for the HB stars we considered. This value (which includes measurement errors, which are however small) is almost coincident with the value of 7.8 ± 0.3 km s^{-1} listed by Harris (1996). Since spectra with the HR03 set up were obtained two years later than those with the other two set-ups, variations in the radial velocity might be used to detect binaries. For two stars (#88 and #62), we obtained differences in radial velocities

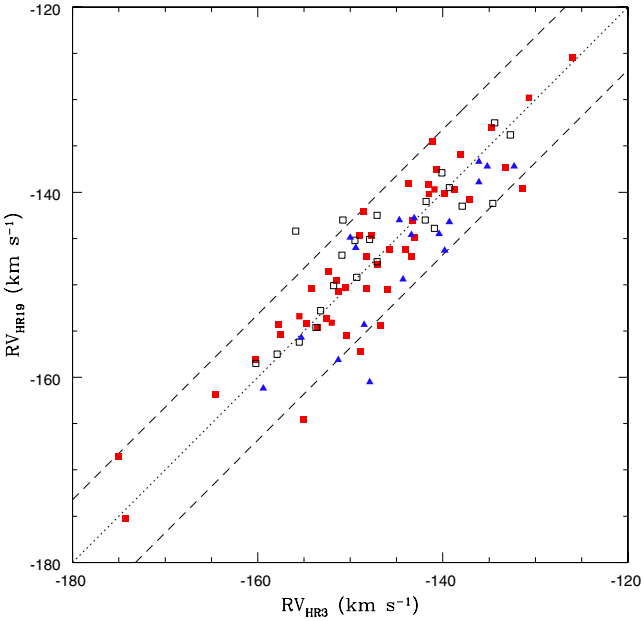

Fig. 2. Radial velocities from set-up HR03 vs. those from set-up HR19A; different colours are for stars of different groups (see Sect. 4): Group 1: red filled squares; Group 2: black open squares; Group 3: blue filled triangles. Dotted line represents equality; dashed lines are ±2 times the observational errors.

of −11.7 and +12.6 km s^{-1}, respectively, when comparing data obtained with HR03 and HD19A. These differences are about 3.5 times larger (in absolute value) than is typical for other stars: they are then candidate binaries. We notice, however, that both of them are quite fast rotators (see next section) and this makes their radial velocity measures more uncertain.

We may compare our radial velocities with those measured by Marino et al. (2013) for the four stars in common between the two samples. On average, the difference (ours–Marino et al.) is 0.3 ± 1.6 km s^{-1} (rms = 3.2 km s^{-1}). Most of the scatter is due to star #17 (for which we do not have the spectra with the HR03 set-up), which is star #166 in their notation. According to their discussion, this star is suspected of being a blue straggler star (BSS). BSS often show radial velocity variations, associated to binarity. If this star is dropped, on average the difference is −1.3 ± 0.2 km s^{-1}, with a very small r.m.s. scatter of only 0.3 km s^{-1}. We do not attribute much importance to the small zero point difference that is typical of observations with different set ups of GIRAFFE/UVES. The very small rms scatter supports our use of radial velocities for membership, internal dynamics, and binary detection. In addition, we have 14 stars in common with Salgado et al. (2013). While they do not claim high accuracy in their velocities, we found excellent agreement with ours, well within the errors they quoted. On average, our radial velocities are lower by 11.1 ± 1.7 km s^{-1}, with an rms of 6.3 km s^{-1} for individual stars, which is much less than their quoted error of ±18 km s^{-1}.

2.2. Rotational velocities

We found that spectral lines of several stars are clearly broader than those of others. This is likely to be due to rotation (see Peterson 1983; Behr et al. 1999; Recio-Blanco et al. 2004). We then measured the full width at half maximum (FWHM) of the spectral lines, which is the convolution of the instrumental profile and intrinsic broadening of the spectral lines. The values we

[1] Available at http://www.eso.org/sci/software/pipelines/

[2] IRAF is distributed by the National Optical Astronomy Observatories, which are operated by the Association of Universities for Research in Astronomy, Inc., under cooperative agreement with the National Science Foundation.

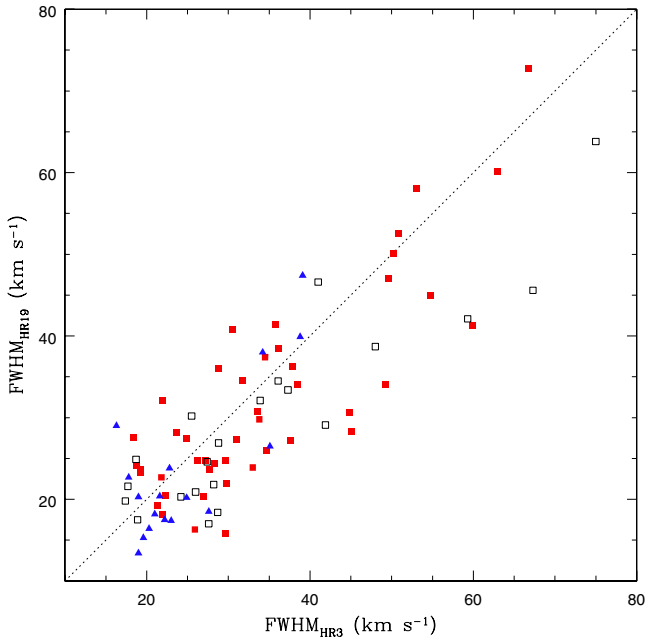

Fig. 3. FWHM of lines from set up HR03 vs. those from set up HR19A; different colours are for stars of different groups (see Sect. 4): Group 1: red filled squares; Group 2: black open squares; Group 3: blue filled triangles.

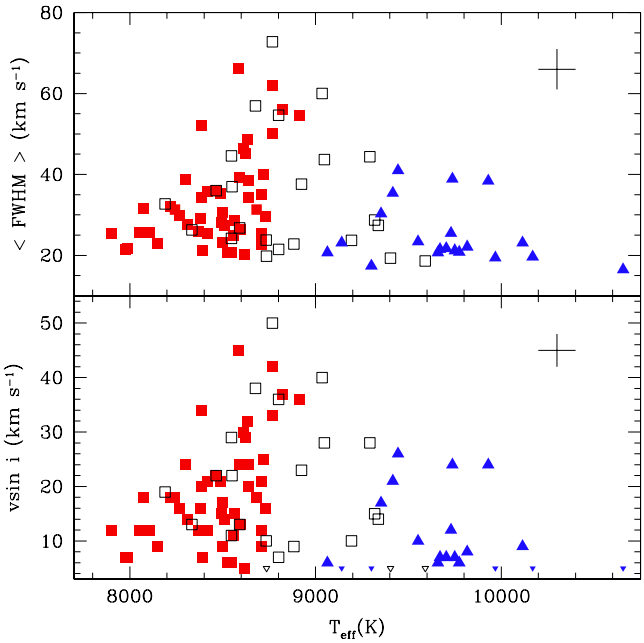

Fig. 4. $T_{\rm eff}$ vs. FWHM of lines (*upper panel*) and rotational velocity (v sin i: *lower panel*); different colours are for stars of different groups (see Sect. 4): Group 1: red filled squares; Group 2: black open squares; Group 3: blue filled triangles. Small triangles in the *lower panel* represent upper limits in v sin i. Typical error bars are also shown.

obtained from individual set ups are listed in Cols. 10–12 of Table 4. The weighted average values (with double weight to results from set ups HR03 and HR19, where there are stronger lines) are given in Col. 13, with their errors in Col. 14. In Fig. 3 we compare the FWHM of lines from set up HR03 to those from set up HR19A. There is quite a good correlation between these measures.

An accurate estimate of the errors in line broadening is complex, because it depends on line strength (hence temperature), S/N of the spectra, and spectral resolution, but this is beyond the scope of our work here. An order-of-magnitude estimate can be obtained by comparing results obtained with different set ups, after taking the different resolving power into account. Typical values are ±5 km s^{-1}. The lower envelope of the distribution (with $FWHM \sim 19$ km s^{-1}) is likely to be populated by slowly rotating star, whose profile is dominated by instrumental broadening and turbulent motions. FWHM of the rotational broadening may then be obtained by deconvolution of the observed FWHM for this value. While our data are not calibrated for this purpose, we expect that for profiles dominated by rotational broadening $v \sin i \sim FWHM/\sqrt{2}$. We then derived values of $v \sin i$ using the formula $v \sin i = \sqrt{(FWHM^2 - FWHM^2_{\rm ins})/2}$, where the second term takes the instrumental profile into account. The values of $FWHM_{\rm ins}$ we used were those appropriate for each set up. Wherever this formula yielded a value of $v \sin i < 5$ km s^{-1}, we only gave an upper limit of 5 km s^{-1} to $v \sin i$. For the four stars in common with Marino et al. (2013), we may compare values of $v \sin i$ obtained with this rough procedure (listed in Column 15 of Table 4) with those they obtained from their higher resolution UVES spectra. On average, the difference (ours–Marino et al. 2013) is $\Delta v \sin i = -2 \pm 3$ km s^{-1} and the r.m.s. scatter of 6 km s^{-1} agrees quite well with our estimate of the errors.

The star with the broadest lines in our sample (#52) has a $FWHM = 73$ km s^{-1}, which corresponds to a rotational velocity of $v \sin i \sim 50$ km s^{-1}. This value is at the upper limit of the distribution for BHB stars (Peterson et al. 1995; Behr et al. 2000a,b; Recio-Blanco et al. 2004; Lovisi et al. 2012).

Figure 4 shows the run of rotational velocities with effective temperatures. At any given temperature, there is some scatter in rotational velocities. The upper envelope of the distribution peaks at about 8800 K. The number of stars with evidence of rotation is a function of temperature: all fast rotators ($FWHM >$ 40 km s^{-1}) are in the temperature range 8400–9400 K.

3. Analysis

3.1. Atmospheric parameters

Our analysis is based on model atmospheres extracted by interpolation within the Kurucz (1993) grid. Interpolations were done as described in Gratton & Sneden (1987) and used in many other papers. The grid of models used for this interpolation does not include any alpha enhancement. However, at this high temperature, most of the electrons are provided by hydrogen, not metals. The impact of modifying model metal abundances is then very small, as confirmed by detailed calculations (see Sect. 3.5).

The most critical parameter in our abundance analysis is the effective temperature $T_{\rm eff}$. In previous papers of this series (Gratton et al. 2011, 2012a, 2013), $T_{\rm eff}$'s were derived from colours using calibrations that, for the BHB stars, were based on Kurucz (1993) model atmospheres. Since red-infrared colours saturate for such warm stars, most useful information is provided by visual and near-ultraviolet colours. Unfortunately, while BVI data were available for all stars, violet colours were only available for about half of them, and we have no reliable UV photometry for a significant number of stars.

A basic problem in deriving colours for the programme stars is the variation in interstellar reddening over the field of M 22. M 22 is seen in projection against the Galactic bulge and has a high ($E(B-V) = 0.34$: Harris 1996) and differential reddening (e.g. Richter et al. 1999). A map of such variation has been

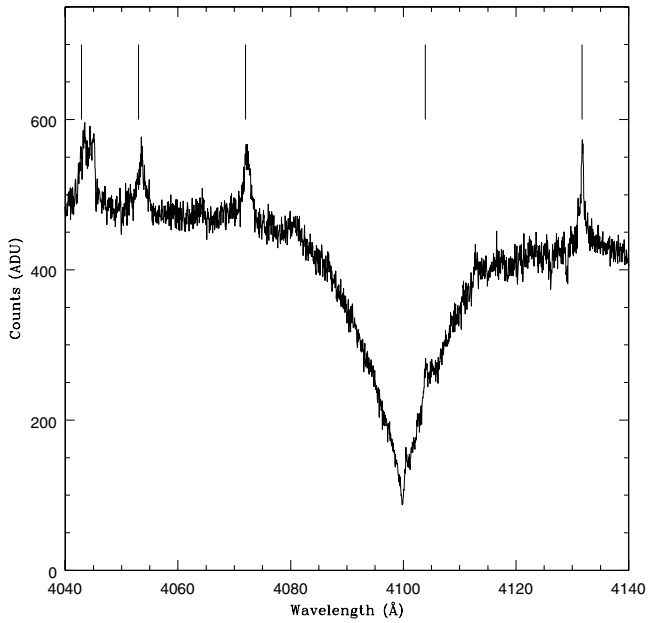

Fig. 5. Portion of the spectrum of star 115 including H_δ. This is the most extreme case of stronger contamination by Th-Ar lines. Identification of several contaminating lines is from the Kitt Peak Th-Ar spectrum (http://old-www.noao.edu/kpno/specatlas/thar/).

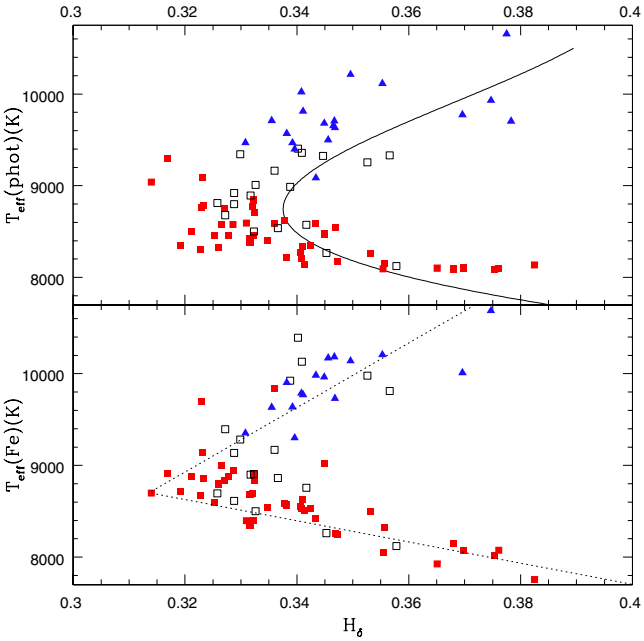

Fig. 6. *Upper panel*: comparison between temperatures from photometry ($T_{\rm eff}$(Phot)) and the index of the strength of the Hδ line (Hδ); overimposed is the relation expected from theoretical models (see Munari et al. 2005). *Lower panel*: the same, but for temperatures from Fe lines ($T_{\rm eff}$(Fe)). Different symbols are for stars of different groups (see Sect. 4): Group 1: red filled squares; Group 2: black open squares; Group 3: blue filled triangles. The fit lines used to define $T_{\rm Cool}$ and $T_{\rm Hot}$ are also plotted in the *bottom panel*.

prepared by Monaco et al. (2004) covering the whole field of interest. We then corrected our colours first for the average reddening of M 22 ($E(B-V) = 0.34$: Harris 1996) and then for the differential reddening provided by Monaco et al. (2004). We then derived temperatures from $B-V$, $V-I$, $b-y$, and $v-y$ colours, reducing them to a consistent scale, which is the one defined by $B-V$ colours. We also considered $V-K$ colours, but later discarded them because errors were too large to be useful. We then made a weighted average of these temperatures, assigning double weight to $v-y$ colours. We called $T_{\rm eff}$(phot) these estimates of the effective temperatures.

These photometric temperatures still contain non-negligible errors, owing not only to errors in the calibration and photometry of individual stars, but also to uncertainties in the differential reddening map, which are of the order of 0.01 mag in $E(B-V)$, which corresponds to several hundred K for BHB stars. Luckily, our spectra offer the opportunity to derive effective temperatures from the strength of H_δ. Hydrogen lines in BHB stars are also sensitive to gravity (see e.g. discussion in Marino et al. 2013); however, this effect does not cause a large scatter in the relation between effective temperature and strength of the line because the spread in mass and radius (and then surface gravity) at a given $T_{\rm eff}$ is actually very small. We then computed an index of the strength of H_δ (which we called by this same name) that is the ratio of the flux within a region 8 Å wide centred on the line and of the average in two similar reference regions located symmetrically with respect to the line at 40 Å separation. We then plotted this H_δ index against $T_{\rm eff}$(phot) (see Fig. 6). For a few stars, contamination of the spectra by the wavelength calibration lamp falsifies this H_δ index, while the spectra can still be used, with some care, for other purposes. This problem was found for nine stars. Figure 5 shows a portion of the spectrum of star 115 including H_δ, which is the case of strongest contamination.

The parameter H_δ shows a smooth run with $T_{\rm eff}$(phot), with a minimum (i.e. strongest line) at about 8800 K. For comparison, we also plotted the observed relation with a calibration based on theoretical models in the upper panel of Fig. 6; for this purpose, we used the same definition of the indices to measure H_δ indices on the theoretical spectral library by Munari et al. (2005). We interpolated the values of the indices we obtained for the observed run of gravity with temperature. On the whole, there is quite good agreement, though measured H_δ index are slightly lower (that is, the line appears stronger) than given by the models. The difference is small and can be attributed to problems in how the continuum normalization was done on our spectra. We attribute the scatter around a mean relation to the effects of residual differential reddening. To support this claim, we constructed another spectroscopic index Fe-Ind that we designated as the logarithm of the sum of the equivalent widths of the three strongest Fe I lines observable in our spectra (at 4045.82, 4063.60, and 4071.75 Å), and also plotted this quantity against $T_{\rm eff}$(phot) (see Fig. 7). We could then fit a straight line through the observed points and construct a temperature index that we called $T_{\rm eff}$(Fe). Plotting H_δ against $T_{\rm eff}$(Fe) (see Fig. 6), we find that the scatter in the plot is considerably reduced. This is precisely what we expect if a significant source of scatter in the $H_\delta - T_{\rm eff}$(phot) plot is due to differential reddening that was not properly taken into account.

We then decided to derive temperatures from the H_δ index. We prefer to use H_δ because we might expect some star-to-star variation in Fe abundances. These were obtained by fitting two straight lines on the $H_\delta - T_{\rm eff}$(Fe) plot: one for stars with $T_{\rm eff}$(Fe) < 8500 K, which we called $T_{\rm Cool}$, and one for stars with $T_{\rm eff}$(Fe) > 9000 K, which we called $T_{\rm Hot}$ (see Fig. 6). The finally adopted temperature from H_δ ($T_{\rm eff}(H\delta)$) was $T_{\rm Cool}$ for $T_{\rm eff}$(phot) < 8400 K; $T_{\rm Hot}$ if $T_{\rm eff}$(phot) > 9750 K; and $T_{\rm eff}(H\delta) = w*T_{\rm Cool}+(1-w)*T_{\rm Hot}$ if $8400 < T_{\rm eff}$(phot) < 9750 K. In this last formula, $w = (T_{\rm eff}{\rm (phot)}-8400)/(9750-8400)$. For

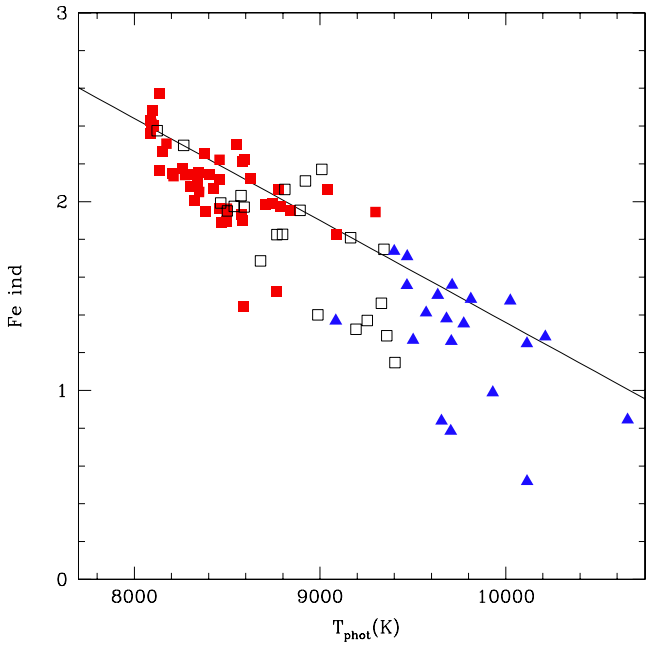

Fig. 7. Comparison between the Fe I line strength index Fe-Ind and temperatures from photometry ($T_{\rm eff}$(Phot)). Different symbols are for stars of different groups (see Sect. 4): Group 1: red filled squares; Group 2: black open squares; Group 3: blue filled triangles. Superimposed is the calibration line we used.

those stars for which no H_δ index could be derived owing to the contamination by the Th-lamp lines, we adopted $T_{\rm eff}$(phot) as best estimates of the effective temperatures.

Figure 8 compares $T_{\rm eff}(H\delta)$ with $T_{\rm eff}$(phot) (as well as with temperatures from individual colours). The correlation is quite tight, with an rms of 144 K. The small residual scatter may be explained by errors in the differential reddening estimates of ∼0.01 mag, which is well within the accuracy of the method devised by Monaco et al. (2004). While such corrections appear small, there was clear improvement on the results from use of $T_{\rm eff}(H\delta)$ rather than $T_{\rm eff}$(phot). We hence assign an error of ±100 K to $T_{\rm eff}(H\delta)$.

Once effective temperatures and differential reddening values were accurately determined, surface gravities $\log g$ can be determined from the location of the stars in the colour–magnitude diagram (after correction for differential reddening) with very small errors, because masses of the stars cannot be very different from an average value of 0.63 $M_\odot$ (see Gratton et al. 2010). To this purpose, we adopted bolometric corrections from Kurucz (1992, for the metallicity of [Fe.H] = −1.70 given by Harris 1996) and a distance modulus of $(m - M)_V$ = 13.6 (Harris 1996). Surface gravities have errors not larger than ±0.05 dex.

More critical is the derivation of microturbulent velocities $v_{\rm t}$. For & Sneden (2010) have shown that the value of $v_{\rm t}$ changes systematically with temperature along the HB, reaching a maximum near the RR Lyrae instability strip. Quite high values of $v_{\rm t}$ are then appropriate for the cooler stars in our sample, while lower ones are more appropriate for hotter stars. Our limited spectral range – hence line list – does not in general allow derivation of reliable $v_{\rm t}$ values, so we adopted $v_{\rm t}$ = 3.0 km s^{-1} for stars with $T_{\rm eff}(H\delta) > 9000$ K, and $v_{\rm t}$ = 3.0–0.6($T_{\rm eff}(H\delta) - 9000$) for cooler stars. However, in about 20% of the cases we had to modify this value, by as much as 1.5 km s^{-1} in the most extreme cases, to reduce the scatter in abundances from individual lines of O I and Fe I. Errors in these estimates of $v_{\rm t}$ are quite large, so we think a value of ±1 km s^{-1} is appropriate.

Finally, we adopted the same model metal abundance of [A/H] = −1.70 (Harris 1996) for all stars. While M 22 is known to have a spread in [Fe/H], this is not greater than 0.25 dex peak to valley (Marino et al. 2011b). An error bar of ±0.2 dex should then be appropriate for [A/H].

We may compare our estimate for temperature and gravity with Salgado et al. (2013) ones for the 14 stars in common between the two samples. On average, there are no systematic differences: the offset (in the sense ours-Salgado et al.) is 93±117 K (rms = 436 K) for temperatures and 0.05 ± 0.07 dex (rms = 0.27 dex) for gravities.

3.2. Equivalent widths

Our abundances rest on analysis of equivalent widths (EW). They were obtained by line integration, and are the average of a manual measure, where line edges and local continuum level were set by eye inspection of the spectra, and of an automatic measure that is a measure of the average of the flux within a band four times the FWHM wide centred on the line (taking the radial velocity of the star into consideration), divided for the average fluxes in two comparison "continuum" regions (each ∼2 Å wide) on both sides of each line. The EWs measured with the automatic procedure were typically slightly lower than those measured manually: $EW_{\rm Auto}$ = 0.872 $EW_{\rm Manual}$ − 6.7 mÅ, with an rms of the differences of 9.7 mÅ. The two sets of EWs were put on a uniform scale by correcting the automatic measures to the manual ones. Figure 9 compares the two sets of EWs.

Care was taken to consider the star-to-star variations in the widths of the lines due to stellar rotation (see previous paragraph). On the other hand, identification of local continuum and line blending are generally not a problem, since very few detectable lines are typically present. In the near infrared, telluric line subtraction is an issue for N and Na lines. It was obtained by dividing the spectra for the average of early type stars with very different radial velocities obtained throughout our programme (see Fig. 10).

Using the Cayrel (1988) formula, we find that the equivalent widths have errors of ±2, ±3, and ±5 mÅ for HR03, HR12, and HR19A spectra, respectively. Errors are up to twice as large for rapidly rotating stars.

3.3. Helium abundances

Following Villanova et al. (2009), we derived He abundances for stars with an effective temperature in the range 9000 < $T_{\rm eff}$ < 11 000 K from the He I line (actually a narrow multiplet) at 5875.6 Å. Figure 11 shows some examples of the He lines. To show them more clearly, we averaged spectra of different stars in bins in temperature. Figure 12 shows the run of the EW of this line with temperature for individual stars. Given the rather low S/N (∼50) of the spectra and the weakness of the He line, He abundances for individual stars have quite large errors.

Marino et al. (2014) present a non-LTE analysis of the He lines in BHB stars of NGC 2808. They also used a different code to synthesize He lines. The average He they obtained for their stars in NGC 2808 is quite high, Y = 0.34 ± 0.01 ± 0.05, where the first error bar is derived from star-to-star scatter, and the second one describes the effects of systematics. Marino et al. determined an He abundance that is consistent with the one used to compute the stellar atmosphere, while in our previous analysis

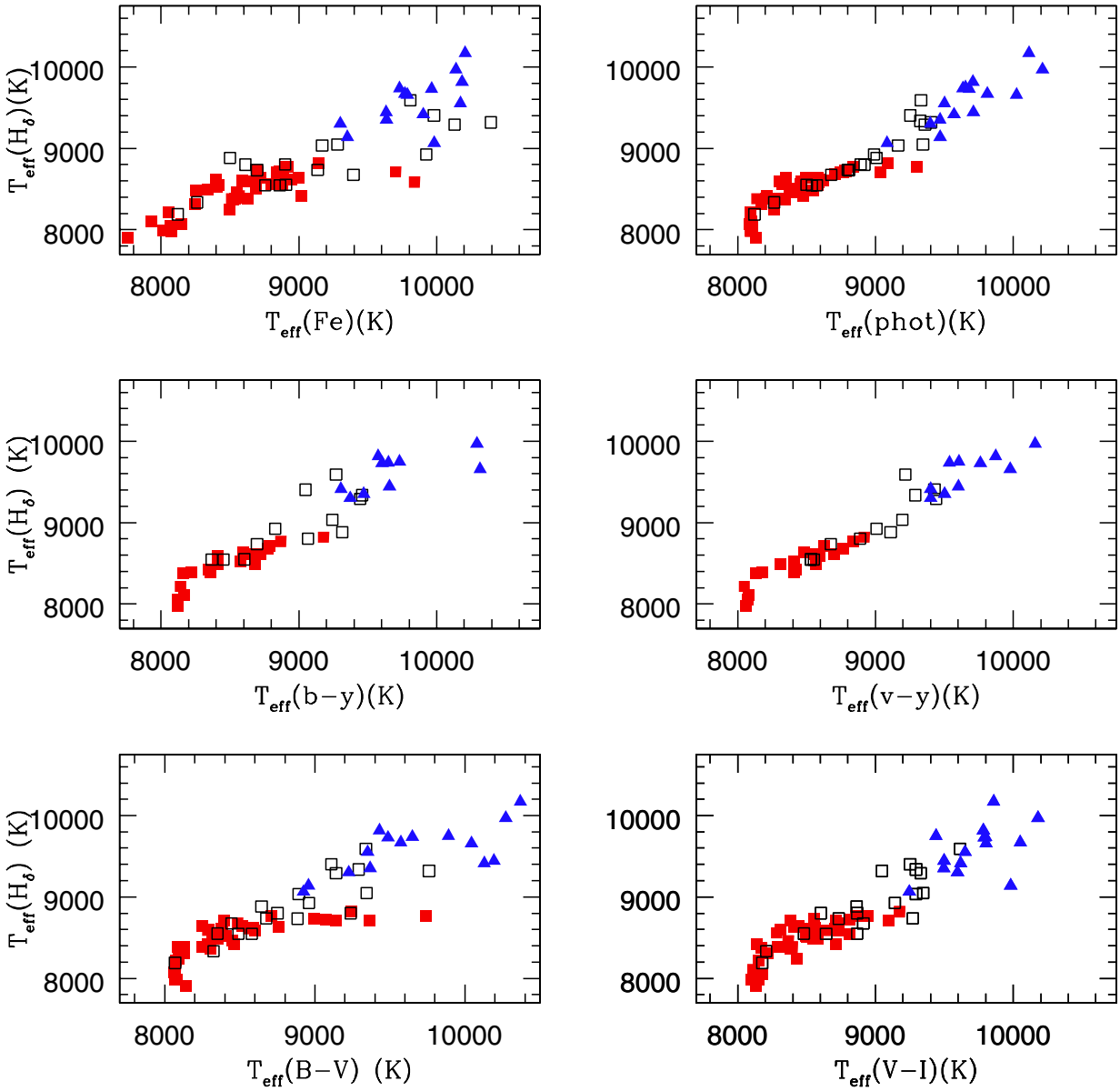

Fig. 8. Comparison between temperatures from colours and their average ($T_{\rm eff}$(phot)) and from our calibration of the Hδ line ($T_{\rm eff}$(Hδ)). Different colours are for stars of different groups (see Sect. 4). Group 1: red filled squares; Group 2: black open squares; Group 3: blue filled triangles.

we assumed He to be a tracer element; that is, the model atmosphere is assumed independently of the He abundance that is derived. Our approach may lead to (unphysical) very large He abundances when the strength of the He line is overestimated due to measuring errors. The error bar obtained using Marino et al. approach is then by far more realistic than obtained assuming it is a trace element. Furthermore, we assumed LTE, while Marino et al. compute full statistical equilibrium calculations. It appears that their methods are superior to those that we used in previous papers of this series, so it is interesting to obtain abundances on their scale.

We do not have access to their analysis code. However, we expect strong regularities in the He abundances when they are derived from the same line in a limited range of parameters, so we proceeded as follows. First, we examined the run of the non-LTE corrections. We found that these are closely related to the EW of the 5876 Å He line and are represented well by a simple linear relation:

$$Y(\mathrm{non-LTE}) - Y(\mathrm{LTE}) = -9.00 \times 10^{-4}\, EW - 0.0192, \quad (1)$$

where the EW is in mÅ. We could correct the helium LTE abundances for NGC6752 (Villanova et al. 2009), M4 (Villanova et al. 2012) using this formula. When added to the results by Marino et al. (2014) for NGC 2808, we thus have a consistent set of He non-LTE abundances for stars over the whole range of temperatures considered.

The He abundances for BHB stars obtained in this way are mainly a function of EW and temperature, with a small correction for surface gravity and an even smaller one for metal abundance. To show this, we constructed a parameter X that is a combination of EW and temperatures:

$$X = 10^{12}\, EW/(T_{\rm eff} - 5000)^{3.9}, \quad (2)$$

and then plotted the values of the He abundance by mass Y against X (see Fig. 13). We found that the points display a very small scatter around a cubic fit through the origin

$$Y = 1.8224\, X + 3.2125\, X^2 - 14.484\, X^3, \quad (3)$$

derived from stars cooler than the Grundahl jump. The rms of the points around this relation is 0.016 in Y.

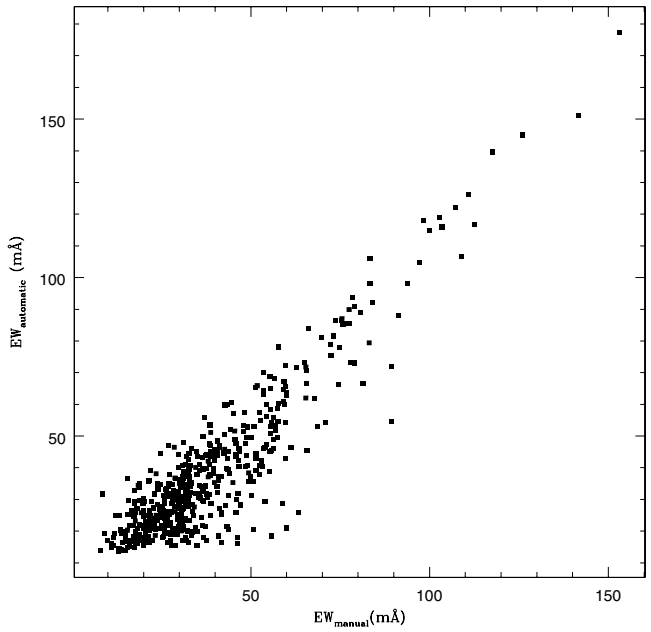

Fig. 9. Comparison between EWs measured manually and by the automatic procedure described in the text. The automatic EWs were corrected for the relation given in the text before being plotted.

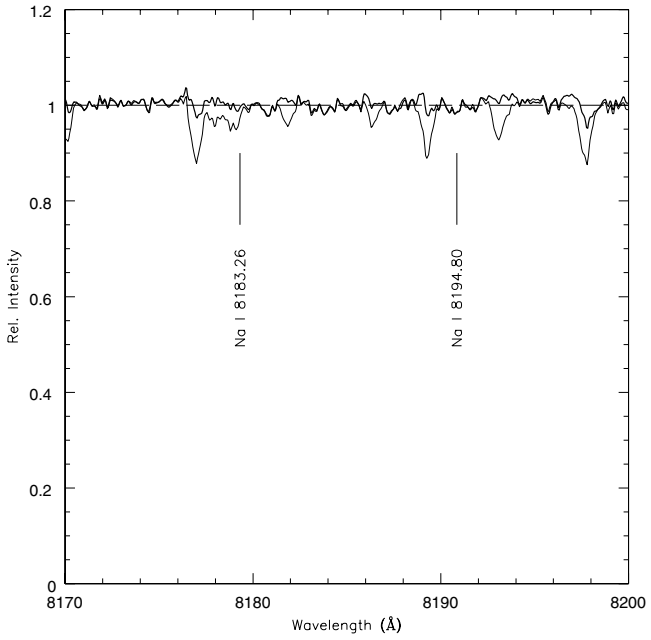

Fig. 10. A portion of the spectrum of star #2 including the Na I doublet at 8183−94 Å before (thin line) and after (thick line) the division for telluric lines. Dashed line is an approximate reference continuum. The Na I lines are very faint, The weakest blue line is not detected; the strongest red one is at the limit of detection.

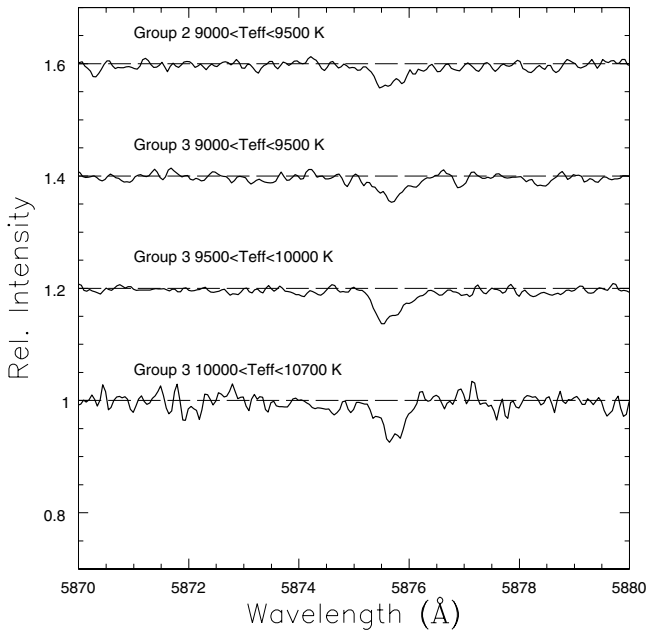

Fig. 11. Average spectra in the region of the He I line at 5876 Å for stars in different temperature bins. See Sect. 4 for the definition of different groups of stars. Spectra have been offset for clarity.

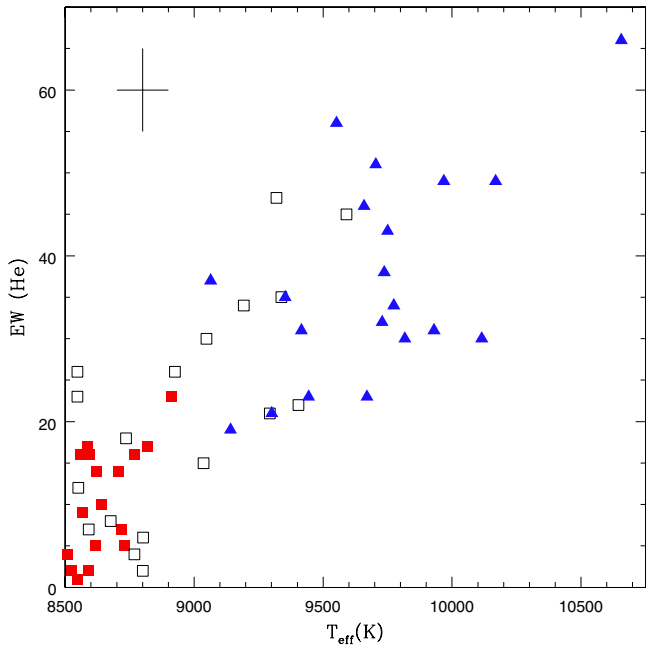

Fig. 12. $T_{\rm eff}$ vs. the equivalent width of the He I line at 5876 Å. Different colours are for stars of different groups (see Sect. 4): Group 1: red filled squares; Group 2: black open squares; Group 3: blue filled triangles. Typical error bars are also shown.

We derived He abundances for M 22 stars using these relations (Col. 2 of Table 6, with errors on the next column), and found an average He abundances by mass of $Y = 0.338 \pm 0.014 \pm 0.05$, where the first error bar is derived from star-to-star scatter, and the second one referring to systematics is simply the one adopted by Marino et al. (2014) for NGC 2808 stars. This value is greater than expected from primordial nucleosynthesis ($Y = 0.248$: Cyburt 2004), even if the effect of first dredge-up is taken into account (the expected surface He enhancement is $\Delta Y \sim 0.015$: Sweigart 1987). This indicates that the BHB stars of M 22 hotter than 9000 K are moderately He-rich.

We notice that the He abundances of the BHB stars of M 22 are not significantly different from those of the BHB stars in the same temperature range in NGC 2808. This result could also be derived immediately by a comparison of the equivalent widths, which on average are similar at a given $T_{\rm eff}$.

To verify that the high He abundances found for the BHB stars of M 22 are not simply an artefact of our procedure, we used the same approach to homogeneously determine

Table 7. Average He abundances from the 5876 Å line for selected clusters.

Cluster	[Fe/H]	Rel. Age (1)	$\log T_{\rm eff}$(HB) Min	$\log T_{\rm eff}$(HB) Median	$\log T_{\rm eff}$(HB) Max	Ref.	$N_{\rm stars}$	$\log T_{\rm eff}$ Range	$\langle Y \rangle$	rms
NGC 1851	–1.18	0.81	3.73	3.74	4.08	2	19	3.95÷4.06	0.297 ± 0.020	0.088
NGC 2808	–1.18	0.83	3.75	3.92	4.57	3	17	3.96÷4.06	0.336 ± 0.013	0.052
M 5	–1.33	0.85	3.76	3.89	4.18	4	15	3.95÷4.02	0.312 ± 0.017	0.064
M 4	–1.18	0.97	3.72	3.76	4.04	5	6	3.95÷3.98	0.295 ± 0.011	0.028
M 22	–1.70	1.06	3.82	3.97	4.22	6	29	3.95÷4.03	0.338 ± 0.014	0.074
NGC 6752	–1.55	1.02	3.82	4.02	4.47	7	4	3.93÷3.94	0.252 ± 0.016	0.031

References. 1. From Gratton et al. (2010); 2. Gratton et al. (2012a); 3. Marino et al. (2014); 4. Gratton et al. (2013); 5. Villanova et al. (2012); 6. This paper; 7. Villanova et al. (2009).

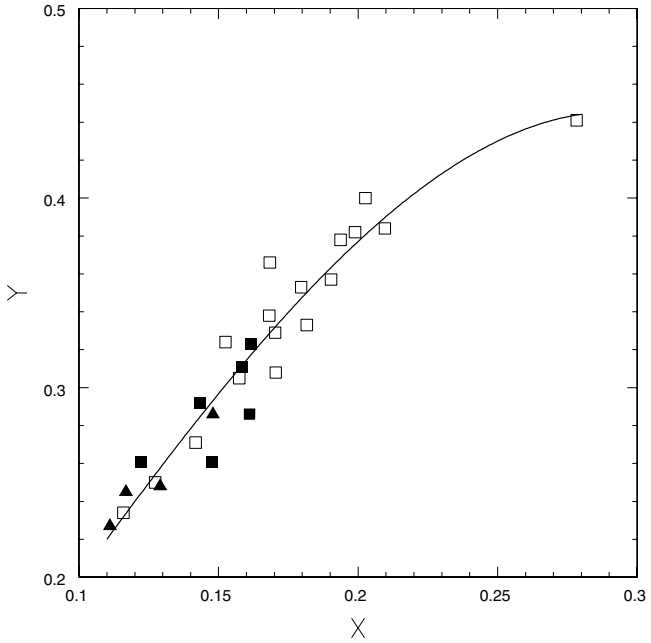

Fig. 13. Relation between the X index for the strength of the He I line at 5876 Å (see Eq. (2) for a definition) and the He abundance by mass Y for BHB stars in NGC 2808 (Marino et al. 2014: open squares), NGC 6752 (Villanova et al. 2009: filled triangles), and M 4 (Villanova et al. 2012: filled squares). He abundances from these two last papers were corrected for departures from LTE and a zero point offset of 0.036 in Y. Overimposed is the best fit cubic through the origin (Eq. (3)).

He abundances from the EW of the 5876 Å line for BHB stars in different clusters (see Table 7). The He abundances for NGC 1851 and M 5 we give here were derived using the formula given in this paper, and are then different from those given in our previous papers. To put these He abundances into a context, we also listed values for the metallicity and relative age of each cluster as listed by Gratton et al. (2010). We also transformed the maximum, median, and minimum colours of HB stars from the same source into minimum, median, and maximum temperature along the HB, and compared these values with the range of temperature of the stars observed in various clusters. These values are listed in Cols. 4–6 of the Table. We also listed the temperature range for the stars for which He abundances were derived. When looking at the He abundances listed in this table, it should be recalled that they do not refer to the whole cluster, but only to those HB stars that happen to be in the right temperature range ($8500 < T_{\rm eff} < 11\,500$ K). Typically, there are stars hotter (and then, possibly more He-rich) and cooler (more He-poor) than the examined stars. Namely, in NGC 1851 and M 4, the stars examined by Gratton et al. (2012a) and Villanova et al. (2012) are among the hottest (and then probably He-rich) in the cluster, while in NGC 6752 they are among the coolest (and then probably He-normal) ones. In all other cases, the HB extends on both sides of the temperature range over which He abundances were determined. A correct interpretation of the result then needs a more detailed modelling for each cluster and consideration of the impact of the first dredge-up.

However, a look at this table indicates that when the observed stars are the coolest along the HB (the case of NGC 6752), we indeed recover an He abundance that is consistent within the errors with the cosmological value. As a result, systematic errors should not be large. On the other hand, there is a wide range of He abundances. In most cases, moderate He excesses with respect to the cosmological values are obtained and are consistent with the location of stars along the HB (see e.g. the discussion by Gratton et al. 2012a and Joo & Lee 2013 for NGC 1851). The values obtained for the stars in M 22 fall at the high extreme of this range, with an average similar to that of the stars of (similar temperature) in NGC 2808. It also agrees well with the value proposed by Joo & Lee (2013) in order to explain colours of HB stars.

We conclude that while systematics errors are possibly not negligible, they should not hamper the conclusion that the BHB stars of M 22 with $T_{\rm eff} > 9000$ K are He-rich. We come back on this issue in Sect. 5.1. We notice that the He abundance we obtained for NGC 1851 is lower than what is obtained for similar stars in NGC 2808, even though the clusters have similar ages and chemical compositions. The difference is significant at about 2σ level even; while this difference might perhaps be attributed to some other difference between stars in these clusters (e.g. different CNO/Fe ratios), we think it needs to be confirmed by more data before any strong conclusion can be drawn.

3.4. Metal abundances

Abundances for other elements are given in Cols. 6–16 of Table 6. As described in Gratton et al. (2011, 2012a, 2013), we obtained O abundances from the high-excitation O I triplet at 7771–74 Åand Na abundances mainly from the D resonance doublet at 5890–96 Å. For a few cool stars we could also detect the higher excitation Na I line at 8194 Å line (after appropriate correction for telluric lines). Consistently with the previous papers, abundances from these lines included non-LTE corrections following Takeda (1997) and Mashonkina et al. (2000).

As we did for NGC 1851 (Gratton et al. 2012a) and M 5 (Gratton et al. 2013), N abundances were also obtained using the high-excitation lines at 8216 and 8242 Å. Analysis of these lines also includes non-LTE corrections, following Przybilla & Butler (2001; see Gratton et al. 2012a) and appropriate correction for

Table 8. Parameter for lines measured on HR03 set up.

Element	Wavelength (Å)	E.P. (eV)	log gf
Mg I	4057.52	4.34	–0.90
Mg I	4167.22	4.34	–0.75
Si II	4128.06	9.83	0.36
Si II	4130.90	9.84	0.55
Ti II	4053.84	1.88	–1.13
Ti II	4163.61	2.58	–0.13
Ti II	4171.86	2.59	–0.29
Fe I	4046.11	1.49	0.28
Fe I	4063.60	1.56	0.06
Fe I	4071.94	1.61	–0.02
Fe I	4132.03	1.61	–0.68
Fe I	4143.88	1.56	–0.51
Fe I	4201.90	1.49	–0.71
Fe II	4173.44	2.58	–2.16
Fe II	4178.86	2.58	–2.44
Sr II	4077.91	0.00	0.15

the contaminating telluric lines. The HR19A set up also allowed Mg abundances to be derived from the Mg II lines at 7877 and 7896 Å. Atomic parameters for all these lines were the same as used in the previous papers. Several more lines were detectable in the blue spectra provided by the HR03 set up (see Table 8); and their oscillator strengths were taken from the NIST database[3].

The use of the LTE approximation for the analysis of these elements may be questioned. For instance, Marino et al. (2013) present both LTE and non-LTE abundances for Fe in their analysis of cool BHB stars in M 22. The non-LTE corrections were very small for Fe II (<0.04 dex, non-LTE abundances being larger) and a bit larger for Fe I (in the 0.2−0.3 dex range, non-LTE abundances being lower). When they applied these corrections, they found consistent abundances from Fe I and Fe II lines.

We found abundances from Fe I lines to be very similar to those from Fe II lines, at variance with the results by Marino et al. (2013). This is not due to differences in temperatures and gravities, which are quite similar in the two analyses; it might rather be due to our adopting much higher values for the microturbulent velocity, because the Fe I lines we used in our analysis are typically stronger than the Fe II lines. Since microturbulent velocities are not derived from first principles, but simply modified in such a way as to obtain agreement between abundances derived from lines of different strength, and since non-LTE corrections are expected to be larger for stronger lines, it is difficult to separate the two effects. Practically speaking, in this case an LTE analysis with a high microturbulence produces abundances similar to a non-LTE analysis with lower microturbulence. Regardless the reason, we find that applying non-LTE corrections as large as those considered by Marino et al. (2013) would destroy the agreement we obtain between Fe I and II abundances, so we prefer not to apply them.

Abundances from the Sr II line at 4077 Å do not include any correction for the increased opacity due to the wings of Hδ; however, we checked that such a correction is very small ($\leq$0.01 dex). Furthermore, no correction for departures from LTE was applied. The size and even the sign of these corrections are not clear. Dworetsky et al. (2008) suggest that they should be small, if any, for population I A-type stars. Similar results have been obtained from statistical equilibrium calculations (Mashonkina et al. 2007; Andrievsky et al. 2011; Bergemann et al. 2012; Hansen et al. 2013) for Sr II lines in metal-poor stars, but these results are only available for $T_{\rm eff}$ < 6400 K, that is for stars much cooler than our programme stars, and small trends are present at the high-temperature, low-gravity extreme of the range of parameters explored in these papers. The abundances of Sr that we obtain are smaller by about 0.5 dex than those by Marino et al. (2012) for subgiants in M 22. The reason for this systematic offset is not clear. On one hand, we notice that the result by Marino et al. is obtained from spectra with moderate dispersion and should then be considered with some caution, their main focus being on the difference obtained for the two SGB branches rather than on the absolute values. On the other hand, we notice that For and Sneden (2010) have obtained a low [Sr/Fe] abundance ratio (on average [Sr/Fe] = −0.30) for field BHB stars from an LTE analysis similar to ours for M 22. The stars they considered have effective temperatures and metal abundances similar to those of the stars we are analysing in M 22, and they adopted similar values for the microturbulent velocities. An even lower abundance of [Sr/Fe] = −0.7 was obtained by Ambika et al. (2004) for a supra-BHB star in M 13. This might suggest a trend toward underestimating Sr abundances in LTE analysis of low-gravity hot stars that might represent an extrapolation of the small trend observed in cooler stars by Andrievsky et al. (2013). Appropriate statistical equilibrium calculations are required to settle this point. However, the effect is not overwhelmingly strong, and we think that our LTE Sr abundances can still be used to separate different groups of stars in M 22 and to internally compare production of elements through the various n-capture processes.

[3] http://physics.nist.gov/PhysRefData/ASD/lines_form.html

Table 9. Sensitivity of abundances on the atmospheric parameters and total errors.

Element	$T_{\rm eff}$ (K)	log g	$v_{\rm t}$ (km s^{-1})	[A/H]	EW (mÅ)	Total
Error	100	0.05	1.0	0.2	5	
Cool BHB star ($T_{\rm eff}$ ~ 8000 K)						
[Fe/H] I	0.084	–0.006	–0.070	0.004	0.060	0.13
[Fe/H] II	0.029	0.013	–0.025	0.004	0.070	0.08
[N/Fe] I	–0.068	0.006	0.038	–0.004	0.113	0.14
[O/Fe] I	–0.006	0.000	–0.164	–0.011	0.064	0.18
[Na/Fe] I	0.033	–0.013	–0.010	0.001	0.119	0.12
[Mg/Fe] I	–0.001	–0.010	0.038	0.003	0.111	0.12
[Mg/Fe] II	–0.054	0.002	0.034	–0.004	0.153	0.17
[Si/Fe] II	–0.098	0.010	0.022	–0.007	0.044	0.11
[Ti/Fe] II	–0.025	0.010	0.026	–0.000	0.061	0.07
[Sr/Fe] II	0.030	0.002	0.000	0.002	0.143	0.15
Hot BHB star ($T_{\rm eff}$ ~ 10 000 K)						
He Y(NLTE)	–0.022	0.013	–0.011	–0.011	0.034	0.05
[Fe/H] I	0.061	–0.017	–0.006	0.009	0.097	0.12
[N/Fe] I	0.013	0.017	–0.010	–0.006	0.075	0.08
[O/Fe] I	0.009	0.018	–0.123	–0.012	0.038	0.13
[Na/Fe] I	0.044	0.000	–0.009	–0.003	0.062	0.08
[Mg/Fe] II	–0.016	0.026	–0.025	–0.009	0.100	0.11
[Si/Fe] II	–0.008	0.035	–0.034	–0.012	0.089	0.10

3.5. Sensitivity of abundances on the atmospheric parameters

The sensitivity of abundances on the adopted values for the atmospheric parameters is given in Table 9. It was obtained as usual by changing each parameter separately and repeating analysis of the abundances. We also considered the contribution to

the error due to uncertainties in the equivalent widths, divided by the square root of the typical number of lines used in the analysis. The values were computed for typical uncertainties in each parameter, as determined in Sect. 3.1. Results are given for two stars (#1 and #129) at the extremes of the observed range of temperatures.

Results for He are for the abundance by mass Y and for the simulated non-LTE analysis of Sect. 3.3. For the other elements, typical uncertainties in the abundances are ±0.1−0.2 dex. In most cases, equivalent widths contribute significantly to final errors. Fe abundances are also affected by errors in the effective temperatures. Since abundances of N I, Mg II, and Si II are not influenced much by temperature for the cooler HB stars, the ratios to Fe abundances have an opposite temperature dependence. Oxygen and, in less measure, Fe abundances are also sensitive to the adopted value for the microturbulent velocity.

4. Cluster analysis and identifications of the main populations

Previous work on M 22 has shown that there are several different populations in this GC. Marino et al. (2009, 2011a,b) find two main populations, each one with a different metal content. These two populations can be well discerned along the RGB and the SGB (see also Marino et al. 2012). Each one of these main populations displays a spread over the Na-O anti-correlation, showing that they have a fine structure (see Marino et al. 2011a,b). Understanding the HB of M 22 requires identifying the progeny of these different populations during the He-core burning phase. To this purpose we should first remember that we did not observe all HB stars in our study. It is then probable that our sample does not represent the whole cluster population.

Our approach was then to identify natural groups among the observed stars. This was done using a statistical cluster analysis. We used the *k-means* algorithm (Steinhaus 1956; MacQueen 1967) as implemented in the *R* statistical package (*R* Development Core Team 2011), where *R* is a system for statistical computation and graphics, freely available on-line[4]. The following parameters were considered when performing the analysis: effective temperatures (to avoid a variance that is too dissimilar to those of other quantities, we used $T_{\rm eff}/10\,000$ K in the analysis) and absolute visual magnitude M_V, which describe the location of stars along the HB; and four parameters describing the chemical composition of the stars (⟨[Fe/H]⟩, [N/H], [O/H], [Na/H]). The first parameters are related to the main subdivisions in metal-poor and metal-rich populations, which are discernible from photometry of the SGB and RGB (Marino et al. 2009, 2012), while the three remaining ones are related to the Na-O anti-correlation.

We found that a subdivision in three groups is able to capture a large fraction of the information, the variance between groups representing 66.7% of the total variance. The three groups are made of 49, 23, and 20 stars. Figure 14 shows the subdivision of the stars into the three groups on the plane of the two principal components. A principal component analysis is the first step of a statistical cluster analysis. The two principal components are defined as follows:

$$PCA1 = 1.11\times10^{-5}\,T_{\rm eff} + 0.151\,M_V + 0.209\,\log n({\rm Fe}) + 0.068\,\log n({\rm O}) + 0.656\,\log n({\rm Na}) + 0.697\,\log n({\rm N})$$

[4] http://www.R-project.org

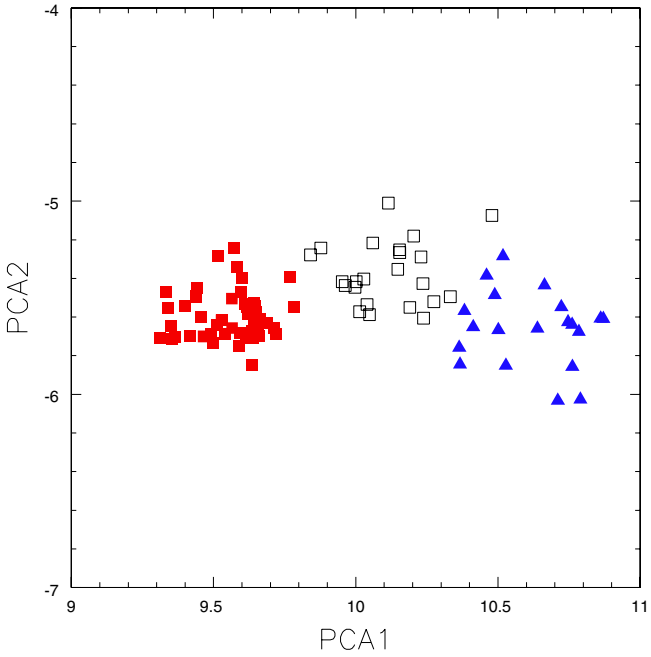

Fig. 14. Subdivision of the stars among the three groups in the two principal components plane. Group 1 stars are represented by red filled squares, group 2 stars by open black squares, and group 3 stars by blue filled triangles.

Table 10. Average parameters for the three groups.

Parameter	Group 1	rms	Group 2	rms	Group 3	rms
$T_{\rm eff}$(K)	8468	237	8860	367	9697	372
Y	..	..	0.363	0.076	0.328	0.072
⟨[Fe/H]⟩	–1.87	0.13	–1.83	0.15	–1.63	0.13
[Sr/Fe] II	–0.54	0.26	–0.54	0.26	–0.18	0.36
[N/Fe] I	0.68	0.15	1.11	0.12	1.06	0.07
[O/Fe] I	0.65	0.12	0.54	0.16	0.54	0.23
[Na/Fe] I	–0.08	0.11	0.20	0.16	0.40	0.17
[Mg/Fe] I	0.73	0.19	0.72	0.11		
[Mg/Fe] II	0.48	0.29	0.59	0.26	0.27	0.31
[Si/Fe] II	0.48	0.19	0.56	0.23	0.32	0.20
[Ti/Fe] II	0.35	0.15	0.43	0.17	0.51	0.15

and

$$PCA2 = -4.70\times10^{-6}\,T_{\rm eff} - 0.262\,M_V - 0.340\,\log n({\rm Fe}) - 0.738\,\log n({\rm O}) - 0.238\,\log n({\rm Na}) + 0.461\,\log n({\rm N}).$$

The main parameters of the three groups are listed in Table 10. The rms for the abundances of the individual groups agree well with the scatter expected for uncertainties in the analysis listed in the last column of Table 9, in agreement with expectations if these groups have a physical meaning. The main driver for the subdivision into these groups is the correlated variations in N and Na abundance, which are responsible for most of the variations in PCA1, and PCA2 is a combination of several parameters with more weight on N and O abundances. Figure 14 shows that the subdivision into groups is driven by PCA1. This means that the subdivision in groups is mainly based on the chemistry. Figures 15 and 16 give the run of the abundances of Fe, Na, N, O with effective temperature, with different symbols for the three groups. The separation is quite evident. Figure 17 gives the same run for the sum of N and O abundances with temperature. The subdivision into groups is still clear. We notice that effective temperature plays a minor role in the definition of PCA1. That there

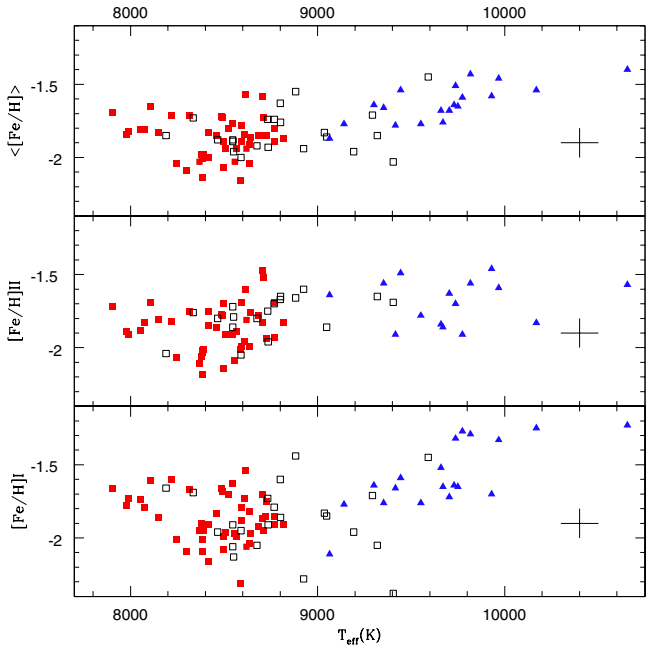

Fig. 15. $T_{\rm eff}$ vs. the abundances from Fe I (*lower panel*), Fe II lines (*upper left panel*), and the average of the two values (*upper right panel*). Different colours are for stars of different groups (see Sect. 4). Group 1: red filled squares; Group 2: black open squares; Group 3: blue filled triangles. Typical error bars are also shown.

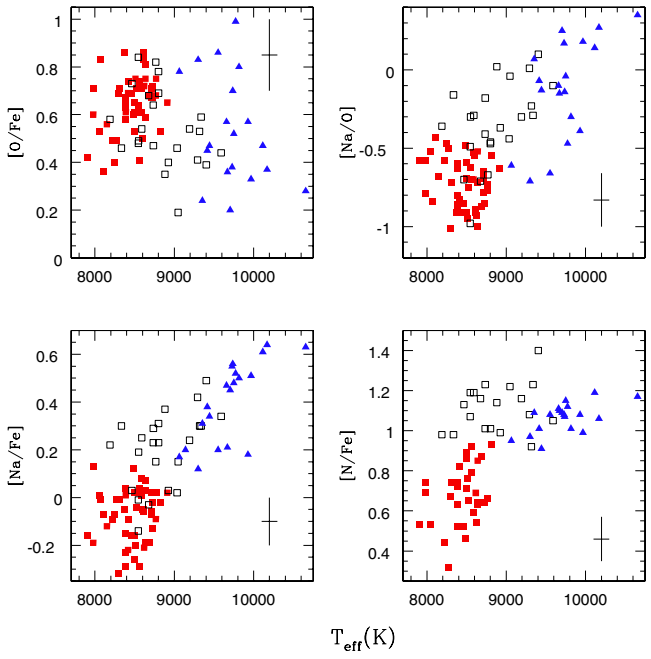

Fig. 16. $T_{\rm eff}$ vs. the abundances of N (*lower right panel*), Na (*lower left panel*), and O (*upper right panel*) and the [Na/O] abundance ratio (*upper left panel*). Different colours are for stars of different groups (see Sect. 4). Group 1: red filled squares; Group 2: black open squares; Group 3: blue filled triangles. Typical error bars are also shown.

is quite a clear segregation of the groups in the colour-magnitude diagram is essentially a consequence of the fact that stars with different chemistry occupy different locations along the horizontal branch. Finally, Fig. 18 compares the Na-O anti-correlation found for the HB stars observed in this paper with the one obtained for the RGB by Marino et al. (2011a).

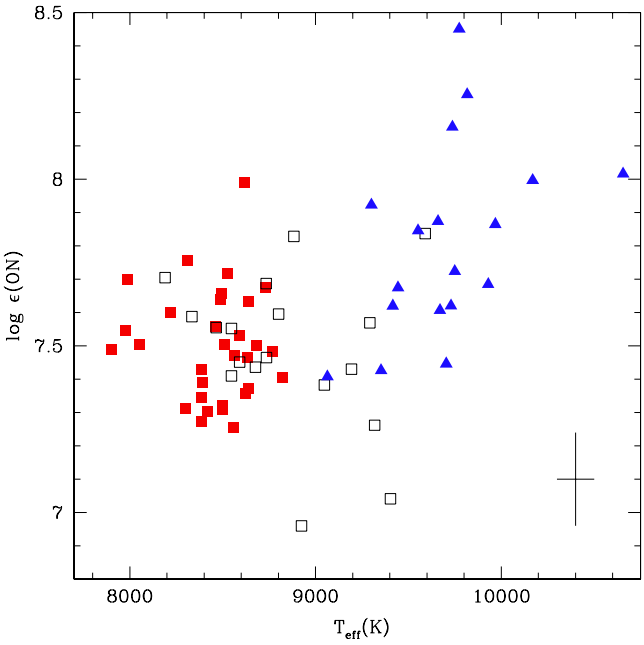

Fig. 17. $T_{\rm eff}$ vs. the sum of N and O abundances. Different colours are for stars of different groups (see Sect. 4). Group 1: red filled squares; Group 2: black open squares; Group 3: blue filled triangles.

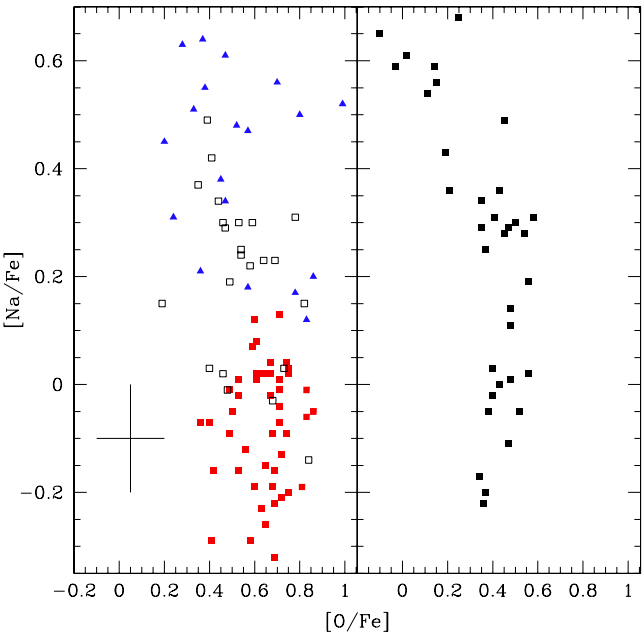

Fig. 18. [O/Fe] vs. [Na/Fe] for BHB stars (*left panel*) and RGB stars from Marino et al. (2011a: *right panel*). In the *left panel* different colours are for stars of different groups (see Sect. 4). Group 1: red filled squares; Group 2: black open squares; Group 3: blue filled triangles. Typical error bars for our analysis are also shown.

From this data, we found that Groups 1 and 2 are made of metal-poor stars. Abundances for these HB stars match the abundances found by Marino et al. (2011a,b) very well for their metal-poor population, and this can be identified with the b-SGB population. We obtained low Sr abundances for these two groups, again in good agreement with the result by Marino et al. The two groups also differ for N and Na abundance, the first group being poorer in these elements than the second one. The low abundances of N and Na of the first group are compatible

with the one for evolved metal-poor giants in the field (see e.g. Gratton et al. 2000). These stars can then be identified with the first (or primordial) population in the cluster. This group is also slightly more O-rich than the second one; however, we did not find any extreme O-poor stars in our sample, while some of them were found by Marino et al. (2011b). We then think that the second group is made of stars that have an intermediate position along the Na-O anti-correlation and that stars strongly depleted in O are not sampled in our analysis because they fall in the region of the HB hotter than the Grundahl jump.

Group 3 is made up of metal-rich stars. Again, the abundances match those found by Marino et al. (2011b) very well for this group of stars, which can be identified with the f-SGB population. We notice that this group is rich in Sr, as found by Marino et al. (2012) for the f-SGB stars of M 22 (although there is an offset between the Sr abundances we obtain for HB stars and those found by Marino et al. for SGB stars; see Sect. 3.4). This group of stars is rich in Na and N, but it is also quite rich in O. We think they can be identified with the less O-poor/Na-rich stars along the Na-O anti-correlation for the metal-rich stars of Marino et al. (2011b). As for the metal-poor stars, Marino et al. (2011b) also find evidence for a metal-rich population strongly depleted in O and very rich in Na. Again, we think that this population is not sampled by our analysis because these stars also fall in the HB-region that is hotter than the Grundahl jump.

We finally notice that stars of both Groups 2 and 3 seem overabundant in He. The result for Group 2 is more uncertain, because it is based on only eight stars that, being not very hot, have quite weak He lines (see Fig. 11). The result for Group 3 is more robust, since it is based on 20 stars that have stronger He lines. However, in both cases the internal scatter is not much larger than expected for the errors listed in Table 9. We then suggest that stars in both these groups are overabundant in He with respect to the cosmological value.

5. Discussion

We intend to make a quantitative comparison between the observed distribution of stars along the HB of M 22 and appropriate synthetic colour-magnitude diagrams, in order to shed light on the properties of the different stellar populations of M 22. This comparison makes use of rough estimates of the frequencies of these different populations that were derived as follows.

First, we recall that our observations are biased because we observe neither the stars hotter than the Grundahl jump nor those in the RR Lyrae instability strip. Owing to the possible presence of radial gradients, it would be important to sample different cluster regions. In fact, Kunder et al. (2013) find a clear indication that stars on the f-SGB are more centrally concentrated than those on the b-SGB in M 22. They did not find any clear trend for HB stars, but in that case their analysis was only limited to the annulus from 4 to 6 arcmin from the centre and a limited number of stars; for reference, the half-light radius of M 22 is 3.36 arcmin according to Harris (1996), and gradients are expected to be clearest when a wide range in logarithm of distance from centre is considered. For practical reasons (avoiding collisions of fibres and contamination by neighbours), most of our stars are at rather large distances from the cluster centre, within an annulus from 1 to 12.5 arcmin, with a median value of 4.0 arcmin. Figure 19 shows that Group 1 looks somewhat less concentrated than Groups 2 and 3. This would agree with expectations and with the result on the SGB by Kunder et al. (2013), because stars of the first generation are usually less concentrated than those of the second generation, and we identified Group 1 with the first generation. However, Kolmogorov-Smirnov tests show that differences between groups are not significant, probably because we only observed a few stars in each group. Since the effect is not overwhelming, we neglect radial variations in this discussion.

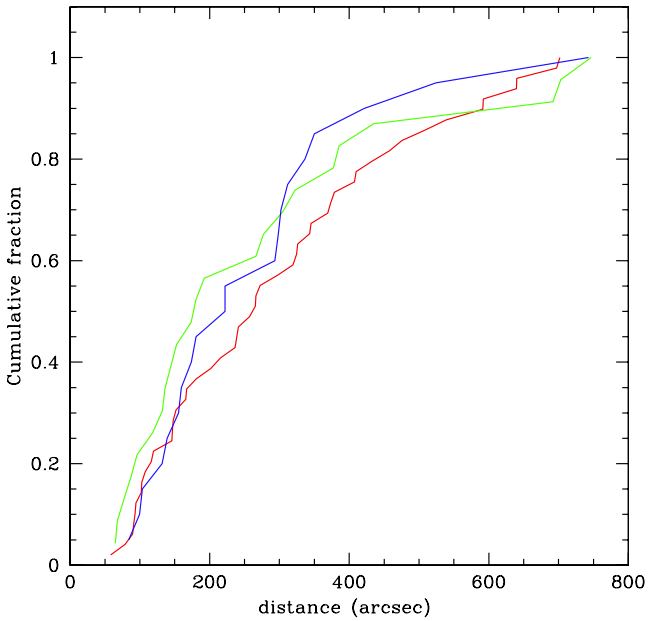

Fig. 19. Cumulative distribution of stars in different groups with separation from cluster centre. Different colours are for stars of different groups (see Sect. 4): Group 1: red; Group 2: green; Group 3: blue.

Table 11. Number of stars of different populations of M 22.

Population	FG	SG-I	SG-E	Total
RGB: Marino et al. (2011a)				
Metal-poor	12	4	5	21
Metal-Rich	–	9	5	14
Frequency over the RGB and SGB (Marino et al. 2011a,b)				
Metal-poor	0.34	0.11	0.14	0.60
Metal-rich	–	0.26	0.14	0.40
BHB: This paper				
Metal-poor	49	23	–	72
Metal-rich	–	20	–	20
Frequency over the whole HB				
Metal-poor	0.39	0.15	~0.14	~0.68
Metal-rich	–	>0.14	~0.14	~0.32

Notes. FG = first generation with primordial composition (normal He, low Na, high O); SG-I = second generation with intermediate composition (moderately high He and Na, moderately low O); SG-E = second generation with extreme characteristics (very high He and Na, very low O).

We then considered the statistics of different groups of stars from the analysis of Marino et al. (2011a). While there are only 35 stars in this sample, there are not strong evolutionary biases because stars with slightly different chemical compositions end up in similar locations along the RGB. They may then give a rough idea of the real frequencies of the main populations. Furthermore, as discussed in the previous section, abundances by Marino et al. (2011a) are on a scale that looks quite similar to what we obtain for the HB stars, so that a direct comparison is possible. Table 11 provides the results of these counts. In this table, FG are O-rich, Na-poor stars that we attribute to the first generation of stars in M 22, and SG-I and SG-E are

second generation with intermediate or extreme values for Na and O abundances throughout the Na-O anti-correlation (see Carretta et al. 2009).

The FG stars are expected to have a He abundance close to the cosmological value; SG-I and SG-E are expected to be moderately and extremely He-rich stars. We then identified our Group 1 with the FG metal-poor population, Group 2 with the SG-I metal-poor population, and Group 3 with the SG-I metal-rich population found on the RGB using data by Marino et al. (2011a).

Using the photometry by Richter et al. (1999), which covers a region within 5 arcmin of the cluster centre with a median of 2.6 arcmin, we found that in their data there are 71 stars hotter than the Grundahl jump (that is, 32% of the total HB stars), 16 stars (7%) in the instability strip, and 138 (61%) stars within the range of temperatures observed by us. These values are consistent with the star counts in the HB by Kunder et al. (2013).

If we make the assumption that stars in the instability strip are the cooler extension of our Group 1, in agreement with the properties of the RR Lyrae in M 22 (Kunder et al. 2013), and are then FG metal-poor stars, we obtain that a fraction of $0.07 + 0.61 \times (49/92) = 0.39$ of the HB stars of M 22 belongs to this population. Within the rather large errors due to small number statistics, this frequency agrees with the one found for this population along the RGB by Marino et al. (2011a). We also note that this group seems to coincide with the group that is redder than the gap at about 9000−9500 K noticed by Kunder et al. (2013) and that makes up 39% of the HB stars of their sample.

We further assume that all SG-I metal-poor stars have temperatures within the range we observed. This is justified by the fact that we do not have any Group 2 star close to edge of this range. In this case the frequency of metal-poor SG-I stars in the whole HB can be obtained by multiplying the frequency in our sample by the fraction of HB stars that are within the temperature range within our sample, that is, $0.61 \times (23/92) = 0.15$.

If we repeat a similar estimate for the SG-I metal-rich stars (identified with our Group 3), we get a fraction of $0.61 \times (20/92) = 0.13$. However, this may be considered more a lower limit than real data, because we may have missed stars of this group because they are slightly hotter than the temperature limit of our survey. This is also suggested by a comparison with the results by Kunder et al. (2013): our intermediate groups (including both Groups 2 and 3) seem in fact to coincide with the clump of stars at the HB position parameter $l_{\rm HB} \sim 26$ in their analysis, which includes some 35−40% of the HB stars of M 22. This is more than the fraction of 0.28 we obtain by summing the stars in our Groups 2 and 3. Also, there are stars in this clump that are clearly hotter and fainter than the stars we observed.

On the other hand, we missed all SG-E stars that make up 28% of the stars along the RGB observed by Marino et al. (2011a). They very likely end up on the HB with temperatures hotter than the Grundahl jump, which are 32% of total according to the Strömgren photometry by Richter et al. (1999). According to Marino et al. (2011a), these hot stars should be roughly equally divided among the metal-poor and the metal-rich populations.

With these assumptions, we obtain the frequencies given in the last part of Table 11. These values should be considered with caution, because they are based on low number statistics. However, on the whole they suggest that some 60−70% of the HB stars of M 22 belong to the metal-poor population and 30−40% to the metal rich one. Given the large uncertainties, these values cannot be considered to disagree with the overall 60−40 subdivision found by Marino et al. (2011a) from RGB stars and a similar rough estimate for SGB stars by Marino et al. (2011b). We notice that a 70−30 subdivision has also been obtained recently by Carretta et al. (in prep.) who consider the bimodal distribution into two sequences along the RGB in the $(y, v-y)$ colours from Richter et al. (1999) photometry, and by Joo & Lee (2013) from a re-analysis of ground-based photometric data by Lee et al. (2009) and of HST-ACS data by Piotto (2009).

We note, in summary:

- All Group 1 stars (roughly 39% of the cluster stars, with 7% cooler than the blue edge of the instability strip) are cooler than 8900 K. They should then have a very narrow mass range, since all are more massive than 0.64 $M_\odot$. For the stars we observed (hotter than the instability strip), the range in mass is from 0.66 to 0.64 $M_\odot$. They should have either all the same He abundance, essentially the cosmological value, or a very narrow range (less than 0.01 in Y).
- Group 2 stars (roughly 15% of the cluster stars) also have a limited range in temperature ($8300 < T_{\rm eff} < 9600$ K), which indicates a very limited range in mass too: $0.63 < M < 0.65$ $M_\odot$. They therefore are likely to all have nearly the same He abundances at $Y \sim 0.015$ larger than Group 1 stars. This value is lower than indicated by the strength of the 5876 Å line.
- All Group 3 stars (roughly 18% of the cluster stars) are hotter than 9000 K. Those stars that we observed are also cooler than 10 700 K; however, there should be hotter stars in this group, up to ∼12 000 K. Depending on the CNO content, this sets an upper limit to the mass, but there should also be a narrow range around it, suggesting a unique value for He abundance. For normal [CNO/Fe], this means $0.60 < M < 0.62$ $M_\odot$ and $Y \sim 0.28$, and for CNO enhanced, this means a range in mass $0.57 < M < 0.59$ $M_\odot$ and $Y \sim 0.30$. Again, this value is lower than indicated by the strength of the 5876 Å line, though the discrepancy is not as large as found for Group 2 stars if CNO is enhanced.
- In addition, there should also be more He-rich stars in M 22, not observed by us because hotter than 10 700 K. They should make up about 28% of the cluster. Using photometry by Kunder et al. (2013), we found that half of them are hotter than 14 000 K, that is, less massive than ∼0.54 $M_\odot$. These stars should be very rich in He ($Y > 0.33$). The other half should have $10\,700 < T_{\rm eff} < 12\,000$ K, and a He abundance of $Y \sim 0.30$.

Based on the previous discussion, we prepared synthetic colour–magnitude diagrams for the HB of M 22. They were performed as described in Salaris et al. (2008) and Dalessandro et al. (2011). We employed the HB evolutionary tracks for [Fe/H] = −1.8 as reference set for the metal-poor stars, and [Fe/H] = −1.6 for the metal-rich ones from the BaSTI database (Pietrinferni et al. 2006). In addition, we have interpolated among the α-enhanced BaSTI models to determine HB tracks for various values of the helium content Y. Finally, we also considered both the reference set and the CNONa anti-correlated models with CNO sum enhanced by 0.3 dex (Pietrinferni et al. 2009). We adopted a distance modulus $(m-M)_V = 13.60$ and $E(B-V) = 0.36$ from Harris (1996).

In our simulations, we have considered as constraints a number ratio between bright (metal-poor) and faint (metal-rich) SGB stars equal to 60:40. We notice that reproduction of the exact details of the colour/temperature distribution requires a lot of fine tuning on the exact parameters. This fine tuning is very time expensive and possibly misleading, because it might lead to

over-confidence on details that may instead depend on the way models were constructed. We then focussed on the main features of such a comparison. We made several attempts to fit both the HB and the other sequences in M 22 (RGB and SGB), changing mass loss and the range of He abundances for the various populations. We find that continuous distributions in He cannot reproduce the segregation between the three groups of stars observed along the HB of M 22. Furthermore, the minimum He abundance of metal-rich stars should be greater than the cosmological value, or else these stars would be fainter (at same temperature) than metal-poor stars, which is not indicated by observations. We then finally assumed the following recipe for the different populations of M 22:

- Metal poor: two subcomponents, the first one (corresponding to Group 1) has a uniform distribution of He in the narrow range $0.246 < Y < 0.251$ and a total average mass lost along the RGB of 0.16 $M_{\odot}$, with a Gaussian distribution with an rms of 0.01 $M_{\odot}$; and a second one (whose cooler part corresponds to Group 2) has a uniform distribution of He in the narrow range $0.285 < Y < 0.319$ and the same total average mass loss of Group 1, but with a narrow Gaussian distribution with an rms of 0.005 $M_{\odot}$.
- Metal rich: a uniform He distribution over the range $0.285 < Y < 0.325$ and a Gaussian distributed total mass loss with average value of 0.160 $M_{\odot}$ and r.m.s. of 0.005 $M_{\odot}$.

We assumed for both the metal-poor and metal-rich HB stellar components an RGB progenitor whose age at the RGB tip is equal to 12 Gyr. Finally, a differential reddening of 0.05 mag (see Kunder et al. 2013) was added to the synthetic data.

We had to assume values of Y that are actually lower than determined from our spectroscopic data for the He-rich populations. In fact, if HB stars were even richer in He than assumed in the models, they would be brighter than observed. Also, we would expect them to be less massive and bluer than observed if they were coeval and lost the same amount of mass along the RGB than the He-normal stars. We conclude that while there is good qualitative agreement between these different helium abundances, there is some disagreement about the exact quantitative level, which is only partly surprising if we consider that they are derived by using completely different and independent techniques.

Figures 20 and 21 compare the synthetic HBs with the observed ones. We notice that this simulation reproduces (i) the ratios between stars within the RR Lyrae instability strip, blueward of it with $M_V < 16$, and in the blue tail, i.e. $M_V > 16$ measured by Kunder et al. (2013), within Poisson errors; (ii) the number ratio between metal-poor and metal-rich stars within the region considered in this paper; (iii) roughly, the segregation of the stars of different groups in the $T_{\rm eff} - M_V$ plane observed in this paper; (iv) the average He abundance of metal-rich stars in the range of effective temperature observed in this paper (the actual value of $Y = 0.29$ is at the lower limit of the range admitted by our data); and the number ratio of metal poor/metal rich stars measured on the SGB by Marino et al. (2009). The scatter in the observed diagram of Fig. 20 looks larger than for theoretical colours. This is largely due to residual photometric errors or some underestimate of the impact of differential reddening. In fact, if we look at the distribution of stars with temperatures of Fig. 21 (where the impact of photometric error and differential reddening is much smaller), the agreement between observation and models is improved.

Answering a question from the referee, we noticed that the scatter in M_V around the mean $T_{\rm eff} - M_V$ relation (~0.10 mag) is

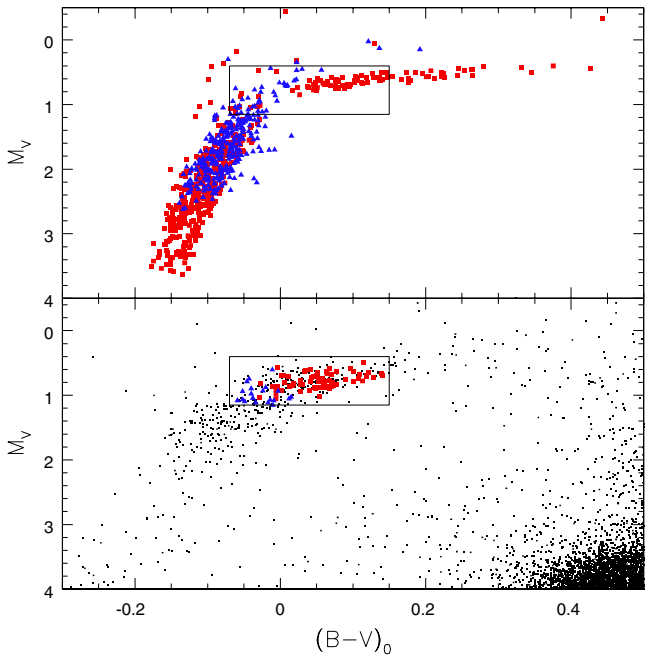

Fig. 20. Comparison between a synthetic (*upper panel*) and an observed (*lower panel*) colour-magnitude diagram for the horizontal branch of M22. Red squares are metal-poor stars (in the *lower panel*, stars of Groups 1 and 2); blue triangles are metal-rich stars (in the *lower panel*, stars of Group 3). In the *lower panel*, stars not observed in this paper are dots. The region of the HB observed in this paper is marked with a rectangle in both panels.

larger than predicted from evolutionary effects (~0.07 mag) for the metal-poor stars, while it is actually smaller than predicted (0.15 vs. 0.18 mag) for the metal-rich ones. The residual errors in differential reddening (~0.01 mag in $E(B-V)$, that is, ~0.05 mag in the residuals in M_V) may explain a part of the larger-than-expected scatter observed for metal-poor stars. Also, errors due to photometry should be considered. Finally, it is possible that the assumptions we made in our population synthesis represents an over-simplification of the real situation in M 22. However, we stress that our comparison only gives a sketch of the real properties of the populations in M 22.

On the whole, this interpretation of the HB of M 22 agrees with what is proposed by Joo & Lee (2013). Details are slightly different, because we find that there should be some overlap between the most He-rich stars of the metal-poor population and the moderately He-rich stars of the metal-rich one. Such fine detailing is only possible here because we have determined the chemical composition of individual stars, while Joo & Lee could only work with photometric data. But excluding this detail, the agreement between ours and their description of the HB of M 22 is impressive.

6. Conclusions

We presented a spectroscopic abundance analysis of a sample of 92 blue HB stars in M 22 in order to discuss the relation existing between chemical composition and the location of the stars along the HB of globular clusters. The stars selected for the analysis are in a restricted range of temperatures between 7800 and 10 700 K. Cooler stars were not considered because they are RR Lyrae variables, while surface abundances for hotter stars are known to be heavily affected by microscopic diffusion and radiative levitation. However, stars in our sample are

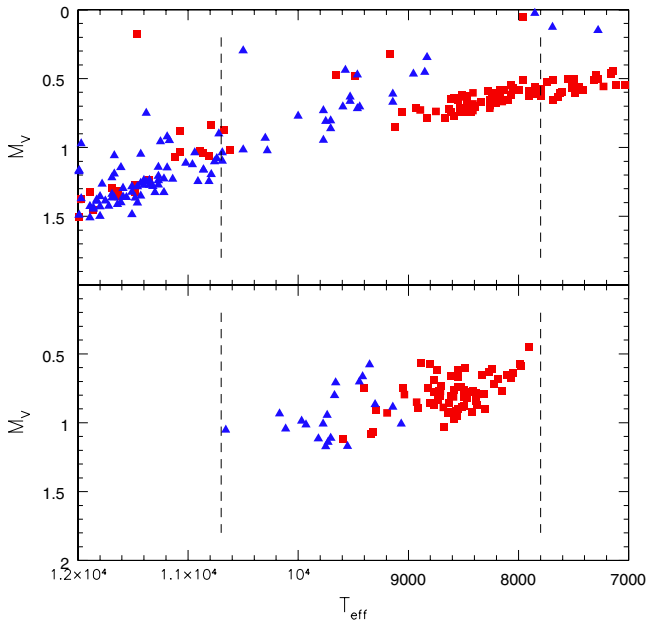

Fig. 21. Details of the comparison between synthetic (*upper panel*) and observed (*lower panel*) $T_{\rm eff} - M_V$ diagram for the horizontal branch of M 22. Red squares are metal-poor stars (in the *lower panel*, stars of groups 1 and 2); blue triangles are metal-rich stars (in the *lower panel*, stars of group 3). The region of the HB observed in this paper is within the dashed lines in *both panels*.

representative of the majority of HB stars in this clusters. We obtained spectra in three spectral ranges, including the stronger lines of Na and O and of the n-capture element Sr. In addition, we were able to derive abundances for He, N, and Fe (from both neutral and singly ionized lines), as well as for other species (Mg, Si, and Ti). Whenever possible, reddening free effective temperatures were obtained from a calibration of the strength of Hδ; otherwise they were obtained from visual and violet colours. Abundances of Na, O, N, and He include non-LTE corrections obtained from literature calibrations. We did not apply non-LTE corrections to Fe abundances because we get agreement between Fe I and Fe II abundances when assuming LTE. This might be a consequence of the rather high values we adopted for the microturbulent velocity, which do, however, agree with determinations for field BHB stars. We get a rather high value for the He abundance, similar to the one recently obtained for similar stars in NGC 2808 by Marino et al. (2014), but higher than in other GCs for which a similar analysis was performed.

We then applied a statistical cluster analysis to our data and found that the stars we studied divide into three groups that occupy adjacent location along the HB, with some overlap. The coolest group is metal-poor, Sr-poor, N- and Na-poor, and O-rich. This result confirms an earlier finding for a few stars by Marino et al. (2013). The intermediate group is still metal-poor and Sr-poor, but is N- and Na-rich, and moderately O-poor. The hotter group is metal-rich and Sr-rich, moderately N- and Na-rich, but also O-rich. These three groups have a clear correspondence with the different populations found on the RGB and SGB by Marino et al. (2011b, 2012): the metal-poor and s-poor population that is also found along the RGB that is the progeny of the b-SGB, and the metal-rich and s-rich RGB one that is the progeny of the f-SGB. We do not find any extremely O-poor star in our sample, but HB stars with this composition are expected to be hotter than the range we observed. Our result then nicely confirms and extends previous investigations and supports the assumption that the spread in colour of HB stars within a GC is mainly determined by variations in the chemical composition, as measured by proxies like Na and O and whenever possible, directly by He lines. We also found that there is not only qualitative agreement between predictions of this scenario and observations, but also a quantitative one; furthermore, star counts in different evolutionary phases agree with each other, supporting the proposed relation between different groups of HB, RGB, and SGB stars.

We found that there should be fairly He-rich stars in M 22, with $Y \sim 0.32$ or even larger, in agreement with what recently proposed by Joo & Lee (2013). These stars should be traceable on the MS of the cluster, once adequate photometric data is available.

Finally, we found several fast rotators. They are concentrated in a narrow region of the HB, with $8400 < T_{\rm eff} < 9400$ K. There is strong correlation between rotational velocity and temperature within our Group 1, which might suggest that fast rotators (where surface rotation is assumed to be a proxy for core rotation, that is the parameter that might be linked to position on the HB) are less massive than slow rotators, as proposed many years ago by Peterson et al. (1983). However, first, the difference in mass is very small ($\leq$0.015 $M_\odot$), so that core rotation is much less important than chemical composition. Second, there is not any similar correlation between temperature and rotational velocity for stars in the other groups. This seems to instead indicate that surface rotation can only be observed in a restricted range of temperatures along the HB of globular clusters. While the lack of significant rotation in cooler stars might be explained by their larger radius and by magnetic braking, we have not an explanation for the slow rotation of the hotter stars (see, however, Vink & Cassisi 2002 for a potential scenario). Further investigation is required to establish that core rotation is indeed related to the colour of HB stars.

Acknowledgements. This publication makes use of data products from the Two Micron All Sky Survey, which is a joint project of the University of Massachusetts and the Infrared Processing and Analysis Center/California Institute of Technology, funded by the National Aeronautics and Space Administration and the National Science Foundation. This research has made use of the NASA's Astrophysical Data System. This research has been funded by PRIN INAF "Formation and Early Evolution of Massive Star Clusters". We thank Philipp Richter for sending us the Strömgren photometric data they obtained for M 22. V.D. is an ARC Super Science Fellow. We thank an anonymous referee for suggestions that helped to improve the paper.

References

Ambika, S., Parthasarathy, M., Aoki, W., et al. 2004, A&A, 417, 293
Andrievsky, S. M., Spite, F., Korotin, S. A., et al. 2011, A&A, 530, A105
Bedin, L. R., Piotto, G., Anderson, J., et al. 2004, ApJ, 605, L125
Behr, B. B., Cohen, J. G., McCarthy, J. K., & Djorgowski, S. G. 1999, ApJ, 517, L135
Behr, B. C., Djorgovski, S. G., Cohen, J. G., et al. 2000a, ApJ, 528, 849
Behr, B. C., Cohen, J. G., & McCarthy, J. K. 2000b, ApJ, 531, L37
Bergemann, M., Hansen, C. J., Bautista, M., & Ruchti, G. 2012, A&A, 546, A90
Carretta, E., Recio-Blanco, A., Gratton, R. G., Piotto, G., & Bragaglia, A. 2007, ApJ, 671, L125
Carretta, E., Gratton, R. G., Lucatello, S., et al. 2010, ApJ, 722, L1
Carretta, E., Lucatello, S., Gratton, R. G., Bragaglia, A., & D'Orazi, V. 2011, A&A, 533, A69
Cassisi, S., Salaris, M., & Irwin, A. W. 2003, ApJ, 588, 862
Catelan, M. 2009, Ap&SS, 320, 261
Cayrel, R. 1988 in The Impact of Very High S/N Spectroscopy on Stellar Physics, eds. G. Cayrel de Strobel, & M. Spite, IAU Symp. (Dordrecht: Kluwer Academic Publishers), 132, 345
Cyburt, R. H. 2004, Phys. Rev. D, 70, 023505
Da Costa, G. S., Held, E. V., Saviane, I., & Gullieuszik, M. 2009, ApJ, 705, 1481
Dalessandro, E., Salaris, M., Ferraro, F. R., et al. 2011, MNRAS 410, 694
D'Antona, F., Bellazzini, M., Caloi, V., et al. 2005, ApJ, 631, 868

Dotter, A. 2013, Mem. Soc. Astron. It., 84, 97
Dworetsky, M. M., Dyer, A., & Persaud, J. L. 2008, Contrib. Astron. Obs. Skalnaté Pleso, 38, 141
Faulkner, J. 1966, ApJ, 144, 978
For, B.-Q., & Sneden, C. 2010, AJ, 140, 1694
Fusi Pecci, F., & Bellazzini, M. 1997, in The Third Conference on Faint Blue Stars, eds. A. G. D. Philip, J. Liebert, & R. A. Saffer (Davis Press), 255
Gratton, R., & Sneden, C. 1987, A&A, 178, 179
Gratton, R., Sneden, C., Carretta, E., & Bragaglia, A. 2000, A&A, 354, 169
Gratton, R. G., Carretta, E., Bragaglia, A., Lucatello, S., & D' Orazi, V. 2010, A&A, 517, A81
Gratton, R. G., Lucatello, S., Carretta, E., et al. 2011, A&A, 534, A123
Gratton, R. G., Lucatello, S., Carretta, E., et al. 2012a, A&A, 539, A19
Gratton, R. G., Villanova, S., Lucatello, S., et al. 2012b, A&A, 544, A12
Gratton, R. G., Lucatello, S., Sollima, A., et al. 2013, A&A, 549, A41
Grundahl, F., Catelan, M., Landsman, W. B., Stetson, P. B., & Andersen, M. I. 1999, ApJ, 524, 242
Hansen, C. J., Bergemann, M., Cescutti, G., et al. 2013, A&A, 551, A57
Harris, W. E. 1996, AJ, 112, 1487
Iben, I. Jr. 1968, Nature, 220, 143
Joo, S.-J., & Lee, J.-W. 2013, ApJ, 762, 36
Kaluzny, J., & Thompson, I. B. 2001, A&A, 373, 899
Kunder, A., Stetson, P. B., Cassisi, S., et al. 2013, AJ, 146, 119
Kurucz, R. L. 1993, CD-ROM 13 (Cambridge: Smithsonian Astrophysical Observatory)
Lee, J.-W., Kang, Y.-W., Lee, J., & Lee, Y.-W. 2009, Nature, 462, 480
Lovisi, L., Mucciarelli, A., Lanzoni, B., et al. 2012, ApJ, 754, L91
MacQueen, J. B. 1967, in Proc. 5th Berkeley Symp., Mathematical Statistics and Probability (University of California Press), 281
Marino, A. F., Milone, A. P., Piotto, G., et al. 2009, A&A, 505, 1099
Marino, A. F., Villanova, S., Milone, A. P., et al. 2011a, ApJ, 730, L16
Marino, A. F., Sneden, C., Kraft, R. P., et al. 2011b, A&A, 532, A8
Marino, A. F., Milone, A. P., Sneden, C., et al. 2012, A&A, 514, A15
Marino, A. F., Milone, A. P., & Lind, K. 2013, ApJ, 768, 27
Marino, A. F., Milone, A. P., Przybilla, N., et al. 2014, MNRAS, 437, 1609
Mashonkina, I. I., Shimanskii, V. V., & Sakhibullin, N. A. 2000, Astron. Rep., 44, 790
Mashonkina, L. I., Vinogradova, A. B., Ptitsyn, D. A., Khokhlova, V. S., & Chernetsova, T. A. 2007, Astron. Rep., 51, 903
Milone, A. P., Stetson, P. B., Piotto, G., et al. 2009, A&A, 503, 755
Moehler, S. 2001, PASP, 113, 1162
Monaco, L., Pancino, E., Ferraro, F. R., & Bellazzini, M. 2004, MNRAS, 349, 1278
Moni Bidin, C., Moehler, S., Piotto, G., et al. 2006, A&A, 451, 499
Munari, U., Sordo, R., Castelli, F., & Zwitter, T. 2005, A&A, 442, 1127
Norris, J. 2004, ApJ, 612, L25
Norris, J., Cottrell, P. L., Freeman, K. C., & Da Costa, G. S. 1981, ApJ, 244, 205
Pasquini, L., Castillo, R., Dekker, H., et al. 2004, SPIE, 5492, 136
Peterson, R. 1983, ApJ, 275, 737
Peterson, R. C., Rood, R. T., & Crocker, D. A. 1995, ApJ, 453, 214
Pietrinferni, A., Cassisi, S., Salaris, M., et al. 2009, ApJ, 697, 275
Piotto, G. 2009, in The Ages of Stars, eds. E. E. Mamajek, D. R. Soderblom, & R. F. G. Wyse, (Cambridge: Cambridge Univ. Press), IAU Symp. 258, 233
Piotto, G., Villanova, S., Bedin, L. R., et al. 2005, ApJ, 621, 777
Przybilla, N., & Butler, K. 2001, A&A 379, 955
R Development Core Team 2011, R: A language and environment for statistical computing, R Foundation for Statistical Computing, Vienna, Asutria
Recio-Blanco, A., Piotto, G., Aparicio, A., & Renzini, A. 2004, A&A, 417, 597
Recio-Blanco, A., Aparicio, A., Piotto, G., De Angeli, F., & Djorgovski, S. G. 2006, A&A, 452, 875
Richter, P., Hilker, M., & Richtler, T. 1999, A&A, 350, 476
Rood, R. T. 1973, ApJ, 184, 815
Salaris, M., Riello, M., Cassisi, S., & Piotto, G. 2004, A&A, 420, 911
Salaris, M., Cassisi, S., & Pietrinferni, A. 2008, ApJ, 678, L25
Salgado, C., Moni Bidin, C., Villanova, S., Geisler, D., & Catelan, M. 2013, A&A, 559, A101
Sandage, A., & Wallerstein, G. 1960, ApJ, 131, 598
Sandage, A., & Wildey, R. 1967, ApJ, 150, 469
Skrutskie, M. F., Cutri, R. M., Stiening, R., et al. 2006, AJ, 131, 1163
Steinhaus, H. 1956, Bull. Acad. Polon. Sci., 4, 801
Sweigart, A. V. 1987, ApJS, 65, 955
Takeda, Y. 1997, PASJ, 49, 471
van den Bergh, S. 1967, AJ, 72, 70
Villanova, S., Piotto, G., & Gratton, R. G. 2009, A&A, 499, 755
Villanova, S., Geisler, D., Piotto, G., & Gratton, R. G. 2012, ApJ, 748, 62
Ventura, P., D'Antona, F., Mazzitelli, I., & Gratton, R. 2001, ApJ, 550, L65
Vink, J. S., & Cassisi, S. 2002, A&A, 392, 553